AD NUMBER
AD360872
CLASSIFICATION CHANGES
TO: unclassified
FROM: confidential
LIMITATION CHANGES
TO: Approved for public release, distribution unlimited
FROM: Distribution authorized to U.S. Gov't. agencies only; Administrative/Operational Use; 09 NOV 1959. Other requests shall be referred to Defense Atomic Support Agency, Washington, DC 20301.
AUTHORITY
DNA ltr, 14 Sep 1995; DNA ltr, 14 Sep 1995

AD 360872L

CONFIDENTIAL

WT-1417

This document consists of 58 pages.

No. 201 of 205 copies, Series A

OPERATION PLUMBBOB

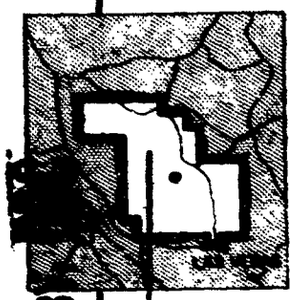

NEVADA TEST SITE

MAY-OCTOBER 1957

Project 2.8

EVALUATION of MILITARY RADIAC (U)

Issuance Date: November 9, 1959

HEADQUARTERS FIELD COMMAND
DEFENSE ATOMIC SUPPORT AGENCY
SANDIA BASE, ALBUQUERQUE, NEW MEXICO

CONFIDENTIAL

Inquiries relative to this report may be made to

Chief, Defense Atomic Support Agency
Washington 25, D. C.

When no longer required, this document may be destroyed in accordance with applicable security regulations.

DO NOT RETURN THIS DOCUMENT

ASC Technical Information Service Extension
Oak Ridge, Tennessee

WT-1417

OPERATION PLUMBBOB—PROJECT 2.8

EVALUATION of MILITARY RADIAC (U)

FOREIGN ANNOUNCEMENT AND DISSEMINATION OF THIS REPORT BY DDC IS NOT AUTHORIZED.

E. J. DiIanni
F. C. Riggin

Naval Material Laboratory
New York Naval Shipyard
Brooklyn 1, New York

U. S. GOVERNMENT AGENCIES MAY OBTAIN COPIES OF THIS REPORT DIRECTLY FROM DDC. OTHER QUALIFIED DDC USERS SHALL REQUEST THROUGH Sponsoring Agency:

Director
Defense Atomic Support Agency
Washington, D. C. 20301

FOREWORD

This report presents the final results of one of the 46 projects comprising the military-effect program of Operation Plumbbob, which included 24 test detonations at the Nevada Test Site in 1957.

For the overall Plumbbob military-effects information, the reader is referred to the "Summary Report of the Director, DOD Test Group (Programs 1–9)," ITR-1445, which includes: (1) a description of each detonation, including yield, zero-point location and environment, type of device, ambient atmospheric conditions, etc.; (2) a discussion of project results; (3) a summary of the objectives and results of each project; and (4) a listing of project reports for the military-effect program.

ABSTRACT

Objectives of Project 2.8 were to (1) develop suitable shields for Navy dosimeter types IM-107/PD (quartz fiber) and DT-60/PD (silver phosphate glass) in order to correct their response to agree with that of standard depth dose detectors imbedded 4 cm in masonite phantoms and (2) compare externally held ratemeter readings with that of a dose-rate standard also imbedded 4 cm in masonite phantoms.

Based on laboratory gamma shielding studies conducted in the range 80 kev to 1.25 Mev, external shields were developed for use with the above dosimeters. The masonite phantoms were designed to simulate average human torso configurations. The effectiveness of the shields in actual field radiological situations was determined in the distributed fields resulting from the induced radiation from Shots Wilson, Priscilla, and Hood and the fallout field from Shot Diablo.

Studies were made of the correlation between dose rates as measured by the AN/PDR-43 (XN-1) and the AN/PDR-44 (XN-1) and the dose rates indicated by the Naval Material Laboratory standard depth-dose ratemeter.

The results of the measurements performed indicate that the laboratory shields provided for the IM-107/PD is adequate to provide good correlation with depth dose. Additional shielding is required for the DT-60/PD. Shielding is needed for the AN/PDR-43 and the AN/PDR-44. Results were similar for both neutron-induced and fallout fields.

PREFACE

The authors wish to acknowledge the cooperation of Frank Day, National Bureau of Standards, for extensive work in the investigation of the energy dependence of the field standards; Paul Caldwell, Naval Research Laboratory, for the fabrication of the phosphate glass needle reader; and George Imirie, Naval Medical Research Institute; J. M. McGreevy, Naval Material Laboratory; T. Sigwurt, New York Naval Shipyard; A. Pfeiffer, Bureau of Ships (Code 916); S. Rainey, Bureau of Ships (Code 348); and G. Mahaffey and staff, Bureau of Ships (Code 854); for their valuable advice and assistance in the preparation and conduct of the field experiments.

CONTENTS

FIGURES

TABLES

Chapter 1
INTRODUCTION

1.1 OBJECTIVES

The overall objective of Project 2.8 was to determine the accuracy provided by several types of Navy radiac equipment in measuring radiological hazard in the field under atomic warfare conditions.

Specifically, the objectives were to: (1) perform a laboratory study to develop suitable shields for dosimeter types DT-60/PD and IM-107/PD to correct their response to agree with the response of the standard depth-dose detectors at a 4-cm depth in simulated human torso configurations (masonite phantoms) and to determine the effectiveness of these shields under field conditions and (2) compare the readings obtained with ratemeter types AN/PDR-43 (XN-1) and AN/PDR-44 (XN-1), when held by a phantom (to ensure shielding and backscattering commeasurate with that resulting from the normal field use of these instruments) with the readings obtained with a "deep"-dose-rate field standard.

1.2 BACKGROUND AND THEORY

The concept of determining the accuracy of information obtained with military radiacs by comparison with a field standard (beta-shielded Victoreen gamma dose meter in air) was first incorporated into the field work of Operation Teapot, Project 6.1.2. The standard used in this operation was designed to measure the gamma dose in roentgen units. In the time which elapsed since Operation Teapot, it has become increasingly evident that this is not necessarily an accurate measure of radiation hazard. Recent biological work (Reference 1) indicates that the physiological effects of a given dose measured in roentgens may vary substantially with the photon energy of radiation. It was shown that corrections should be applied to the roentgen unit at low photon energies, since a dose indication in roentgens at these energies would always be somewhat higher than the biologically significant dose. Furthermore, good correlation has been found between lethality in laboratory animals and the deep gamma dose; that is, the ionization measured several centimeters below the surface of the skin. Separate criteria for the surface or beta dose have also evolved recently. It has thus become important to redesign the field standard apparatus used in the evaluation of military radiacs and to extend the measurements made during Operation Teapot to encompass these biological concepts.

Prior to Operation Redwing, Project 2.7.2, (Reference 2), it was recognized that of the possible doses (air dose, surface dose, 5-cm dose, midline dose, etc.) which could be considered in a residual field, the measurement of the dose received at a depth offered the best chance of correlation with physiological damage. In substantiation of this, the following considerations were given: (1) Measurement of the air dose implies replacement of the body by an instrument in free air at that point (practical only in a laboratory case). (2) A comparatively large surface dose, which could cause little acute biological effect, would occur in residual fallout fields where the surface-to-depth-dose ratio is often 20 to 1 higher (Reference 3).

The dose selected for the Redwing measurements was that measured in a masonite "phantom

man" at a depth of 3 to 5 cm. This depth dose was selected because: (1) The National Bureau of Standards (NBS) Handbook 59 (Reference 4) states that acute effects of radiation are due to damage to the bone marrow whose average body depth is 5 cm. (2) The experimental work of Chambers, et al, (Reference 5) and Imirie and Sharp (Reference 3) has shown that the dose received in a symmetrical residual fallout field is constant, within approximately 10 percent, at all depths further than 3 cm, as opposed to a rise between 3 cm and the surface of a factor of about 20 to 1.

Because of the nondirectionality of radiation, the complex beta and gamma ray spectra, and the geometry presented by an individual in a radiation field, it becomes exceedingly difficult to calculate the tissue dose received from readings of an air or surface dose. Because of this, measurements of the radiation received at a depth have been made by various investigators. Since it has not been feasible to make these measurements in humans, various substitutes have been used. Since water is the predominant constituent of tissue, it has been used as a tissue equivalent medium, and the water bath has been used as a phantom man. Because of practical considerations, the water phantom is not always convenient or suitable for use in measuring depth dose, and many materials, among them rice, powered materials, wax, and pressed woods (masonite), have been studied to find a suitable substitute whose density and atomic number equal those of water (Reference 6). Masonite, a cellulose material, has been found to be a suitable replacement for water and has been used extensively in previous field tests (References 2, 3, 5, and 8) in various shapes and sizes. The phantoms used by Project 2.8, Operation Plumbbob, are of the same type as those used during Operation Redwing, Project 2.72, and are described in detail later in this report.

The results obtained from Operation Redwing showed that the military dosimeters DT-60/PD (silver phosphate glass) and IM-107/PD (quartz fiber), when reading a surface dose, exhibited wide differences, and that neither were in good agreement with standard dosimeters (shielded phosphate glass needles) imbedded in phantoms at a depth of 3 to 5 cm. The wide and varying differences obtained between the surface and depth readings indicate that an error exists in any attempt to measure and interpret the radiation dose received by personnel in a distributed field. It was the aim of this project to extend the work started in Operation Redwing in order to correct the reading errors obtained with the above dosimeter types; and further, to include in the overall experiment, comparison studies of the readings obtained with the Navy ratemeter types AN/PDR-44 (XN-1) and AN/PDR-43 (XN-1) with readings of depth-dose rate for the residual-induced and fallout fields of the type resulting during Operation Plumbbob.

Data was obtained from four shots, which represented two types of residual fields. The fields present following three shots were composed of the neutron-induced activities of Na^{24} and Mn^{56}. The field present following the fourth shot was entirely due to fallout. For the case of the induced fields, the Redwing effects noted in the dosimeters (beta sensitivity and backscatter) were minimized since: (1) the beta radiation was negligible in comparison to the fallout type of field and (2) the gamma energies were higher, thus backscatter was reduced.

However, the design changes indicated by Operation Redwing, i.e., increased shielding of both the standard dosimeter types required field prooftests in induced fields as well as in fallout fields. Since both type of fields were encountered during Operation Plumbbob, a complete evaluation of the shielded dosimeters was possible.

The discrepancies noted by Project 2.72, Operation Redwing, between readings of the surface and depth detectors are considered to be due to a combination of backscatter and incident high-energy beta-radiation effects, both of which tend to increase the readings of the surface dosimeters. In all cases cited, the agreement between the DT-60/PD's and the depth-dose detectors (Reference 2), while not good, was significantly better than the agreement obtained between the IM-107/PD's and the depth-dose detectors. This is attributable to the added shielding provided by the case and the energy-correction shields surrounding the DT-60/PD's. Under Project

2.8, Operation Plumbbob, metallic shields for the two dosimeter types had been designed in the laboratory in an effort to correct their responses to agree with the response of the depth-dose detectors.

In the field, the dosimeters, some selectively shielded, were mounted on the surface of the masonite phantoms and racks, and their readings were compared with the depth readings measured by the imbedded phosphate glass needles. The ratios obtained should allow evaluation of (1) the corrective measures developed in the laboratory and (2) the performance of military dosimeters in induced and fallout residual fields of the types resulting from Operation Plumbbob. It was recognized that for the induced fields, the quality of radiation would differ from that obtained in a fallout field and that lower-energy radiation would be absent.

Chapter 2
PROCEDURE

2.1 OPERATIONS

The project participated in four shots. Chronologically, they were Shots Wilson, Priscilla, Hood, and Diablo. The residual fields encountered in the first three resulted from the neutron-induced activities in the soil. These were identified as being primarily the activities of Mn^{56} and Na^{24} isotopes. The residual field present after Shot Diablo was entirely fallout.

2.1.1 Shot Wilson. At approximately 45 minutes after detonation of the Wilson device, the following equipment was transported into the field and located at positions where the field strength (as measured in air) was of the order of 50 r/hr:

1. Two masonite phantoms loaded with standard depth-dose detectors and with DT-60/PD and IM-107/PD dosimeters (Figure 2.1). These detectors are fully described in Sections 2.2.1, 2.2.2, and 2.2.3. In this report this type of phantom will be designated as the "dosimeter phantoms."
2. One masonite phantom holding both an AN/PDR-43 (XN-1) (Section 2.2.6) and AN/PDR-44 (XN-1) (Section 2.2.7) ratemeter. The phantom was also equipped with a standard depth-dose ratemeter (Section 2.2.8) with its detecting element imbedded in the phantom. This type of phantom will be referred to as the "ratemeter phantom" (Figures 2.2 and 2.4).
3. A masonite rack assembly (Figure 2.3) consisting of four masonite (36 by 8 by $4\frac{1}{2}$ inches) sections on a wood mounting frame. The rack assembly is fully described in Section 2.2.5. The IM-107/PD and DT-60/PD dosimeters were mounted on the surface of the four masonite sections, while the glass needles were imbedded at a depth of 4 cm inside the masonite blocks.

After being exposed for approximately 53 hours, the phantoms and rack were recovered. The instruments were read and the data interpreted in the quonset area following recovery.

2.1.2 Shot Priscilla. At H + 2 hours after Shot Priscilla, one dosimeter phantom and one ratemeter phantom were located at positions where the field distribution was fairly uniform, and the field strength (as measured in air) was between 10 and 20 r/hr. Recovery was made 52 hours after placement, and readings were then taken and interpreted.

2.1.3 Shot Hood. Two hours after Shot Hood, two dosimeter phantoms, one ratemeter phantom, and the dosimeter rack were located in a 2-to-3-r/hr field. Location in this low-intensity field was due to an erroneous AN/PDR-43 (XN-1) reading. About 30 minutes later, the dosimeter phantoms and rack were moved to a 7-r/hr field. It was not feasible to move the ratemeter phantom to a more-intense field, as the power trailer serving the ratemeter recorder was being shared with another project and could not be moved. Recovery of the ratemeter phantom was made at H + 32 hours and recovery of the dosimeter phantoms and rack was made at H + 56 hours.

2.1.4 Shot Diablo. About H + 2 hours following Shot Diablo, two dosimeter phantoms, one rack assembly, and a ratemeter phantom were placed in a field of approximately 50 r/hr. Although the ratemeter reading on the hard-surface road leading toward ground zero had been only 5 r/hr, immediately off the road the dose rate jumped to 50 r/hr. The equipment would have been removed to a lower field, but the truck transporting the instrumentation became im-

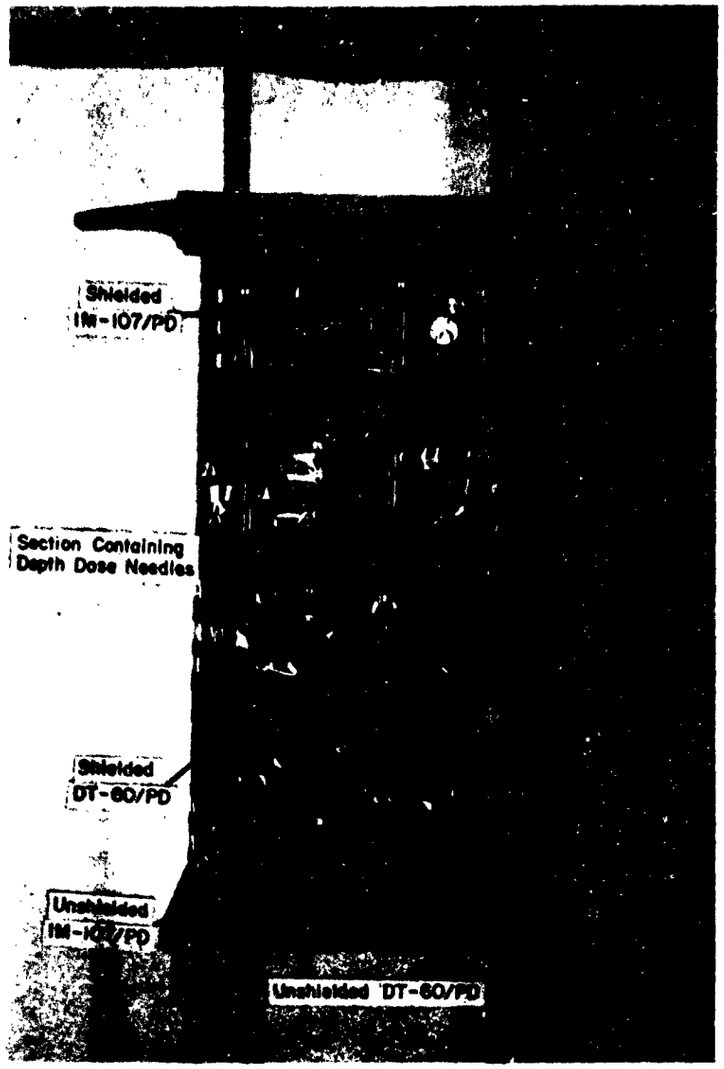

Figure 2.1 Masonite phantom, showing dosimeter array.

Figure 2.2 Masonite phantom loaded with standard depth-dose ratemeter and holding ratemeter Types AN/PDR-43 (XN-1) and AN/PDR-44 (XN-1).

bedded in the sand and could not be moved. Therefore, the instrumentation was installed as rapidly as possible and the personnel evacuated by jeep. Recovery of the dosimeter racks and the dosimeter phantoms was made at H + $6\frac{1}{2}$ hours. The ratemeter phantom was recovered at H + $30\frac{1}{2}$ hours.

2.2 INSTRUMENTATION

2.2.1 DT-60/PD–CP-95/PD System. The DT-60/PD dosimeter (Figure 2.5) contains a sensitive glass square mounted in a lead-lined plastic case (Reference 11). The dosimeter is

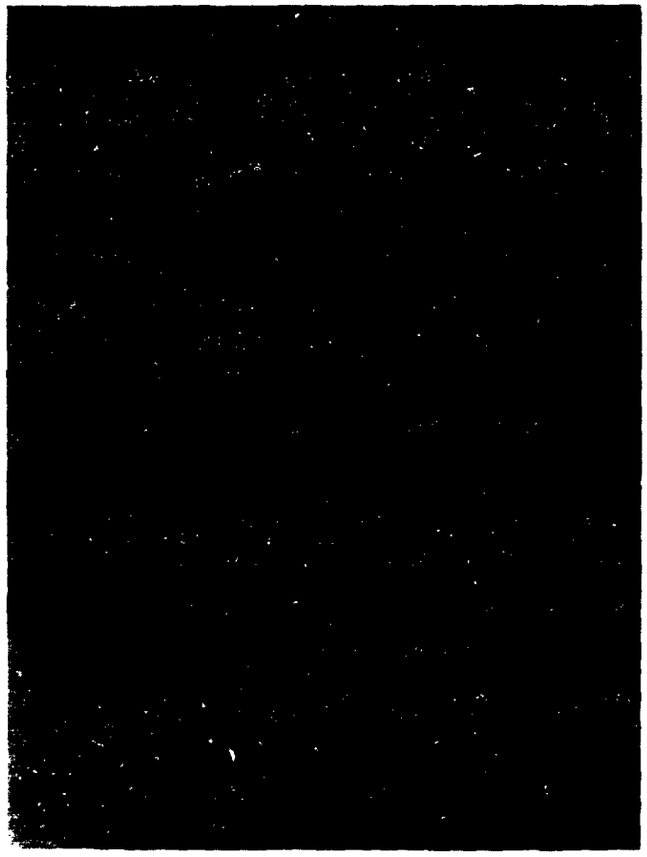

Figure 2.3 Rack containing masonite sections showing dosimeter array.

manufactured by the Corning Glass Works and is a standard stock item in both the Navy and the Air Force. The sensitive glass square, which contains 8 percent silver phosphate, becomes fluorescent in direct proportion to the amount of radiation to which it has been exposed. The dosimeter has a nominal range of 600 r, the reader being the limiting factor.

The CP-95 PD reader (Figure 2.5) is a fluorometer containing an ultraviolet light source to stimulate the silver fluorescence and a photomultiplier to measure the intensity of the fluores-

Figure 2.4 Layout of phantoms and associated equipment.

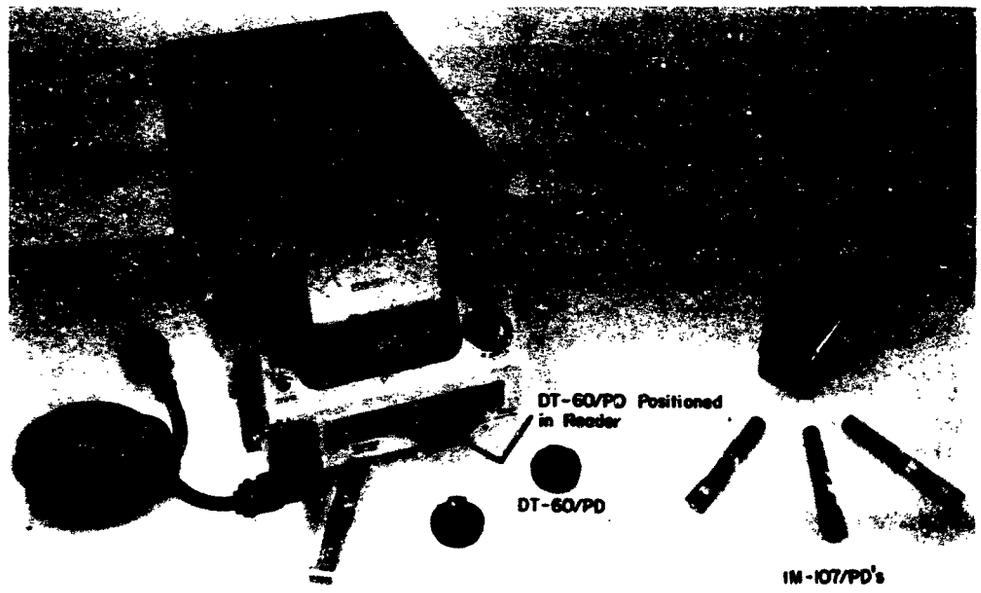

Figure 2.5 Surface dosimeters used on phantoms and CP-95/PD reader for DT-60/PD's.

ence. The reader scale is calibrated directly in roentgens, and the dosimeter-reader combination is designed to have an accuracy of approximately ± 20 percent for gamma energies from 80 kev to 2 Mev. Unused DT-60/PD's drawn from stock have an average pre-dose value of 37 r, which is automatically subtracted by the reader to give a net total exposure.

An investigation of the accuracy of a large random selection of DT-60/PD's indicated a wide variation in the accuracy of the individual instruments, although for the most part the dosimeters read within the specified limits. Since it was felt that the data desired might be obscured by the inherent variation in the DT-60/PD's, an attempt was made to calibrate the individual response of instruments prior to their use. Approximately 700 dosimeters were given an accurate dose of 100 r. As the result of this evaluation, 150 dosimeters whose accuracy was within ± 5 percent were selected for use in the laboratory phase of this work. Due to limitations in time and in the availability of instruments, the dosimeters used in the field were not evaluated in this manner, and for this reason represent the normal stock quality item. As indicated previously, the accuracy of such instruments is quoted as ± 20 percent.

Thirty DT-60/PD's were mounted on each dosimeter phantom, and 64 were mounted on the rack assembly (16 per individual rack).

2.2.2 IM-107/PD. The IM-107/PD is a 0-to-200-r quartz-fiber electroscope manufactured by the Bendix Aviation Corporation (Figure 2.5). It is energy independent above approximately 35 kev, has very low leakage, and is quoted as being accurate to within 20 percent over its entire range (Reference 7).

The dosimeters, although designed to indicate gamma dose, were found to be sensitive to beta radiation during Operation Redwing (Reference 2).

The IM-107/PD's were selected for accuracy prior to use in the field. Of 200 dosimeters tested, 80 were selected that had an indicated accuracy of ± 5 percent, and 30 others showing an accuracy of ± 10 percent were also used.

Forty of the IM-107/PD's were positioned on each dosimeter phantom, and 68 were mounted on the rack assembly (Figures 2.1 and 2.3).

2.2.3 Silver Phosphate Glass Needles and Reader. The glass needles used as the depth-dose standard dosimeters in this project were made of the same 8 percent silver phosphate glass used in the DT-60/PD. The needles are very small, measuring 1 by 6 mm, and were developed by the Naval Research Laboratory (NRL). At present the needles are fabricated by Bausche and Lomb. In the original design, the needle was encased in a cylindrical teflon sleeve whose ends were capped with lead shields (Figure 2.6). A 0.2-mm gap existed between the inside edges of the two lead caps when the dosimeter was assembled. In this configuration, the response of the needle was supposed to have been energy independent from 80 kev to 2 Mev. Needles with this type shielding were used during Operation Redwing. A postoperational evaluation of the Redwing needles and shields by the NBS indicated that a response of 4 percent above normal existed at an energy of 250 kev. To correct for this error, new shields were developed by the Naval Material Laboratory (NML). The changes involved were the increase of the base and wall thickness of the lead caps by 1 mm and the reduction of the gap between the caps to 0.1 mm. As a result of these modifications, the error at the 250-kev energy was reduced so that the response was within ± 10 percent of the average response of the instrument over its energy range. The energy-dependence characteristics of the needles with shield are shown in Figure 2.7.

Improved shields, consisting of a molded gold-polyethylene structure, have been developed by Frank Day of the NBS. These shields extend the energy independence characteristics to a lower limit of 30 kev and provide a uniform response for a dose from 4 π irradiation. Despite the fact that negotiations had been made to procure this type of shield, the contractor was unable to produce them in time for use in the field.

Figure 2.6 Phosphate-glass needles and shields.

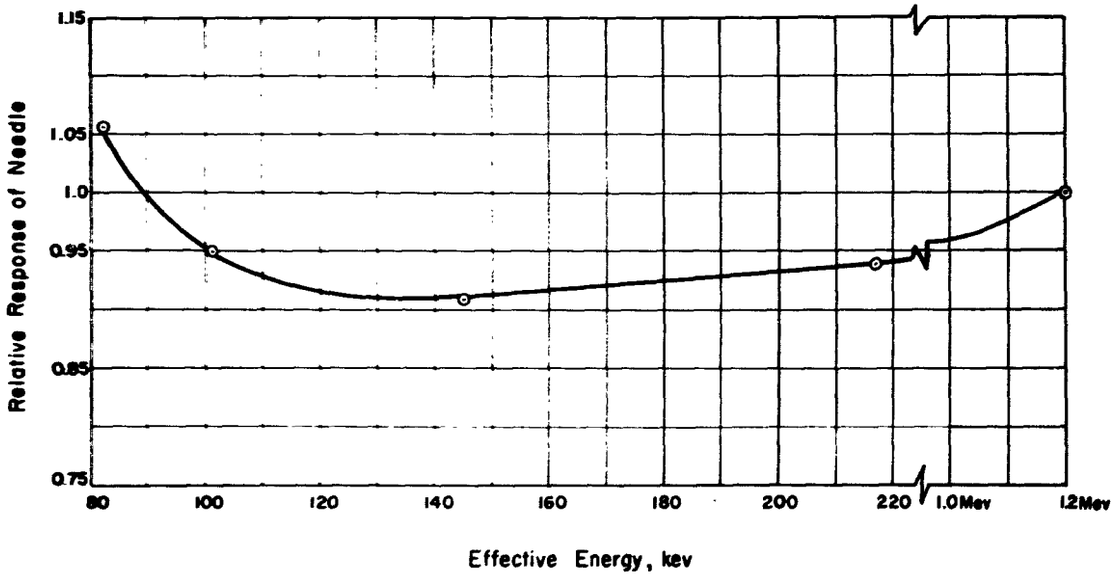

Figure 2.7 Energy-dependence curve of shielded phosphate-glass needles in free air.

The reader (Figure 2.8) for the needles operates on the same principle as that used with the DT-60/PD dosimeters. It was developed by the NRL for use by Redwing Project 2.72. Figure 2.9 shows the calibration curve obtained with a set of ten needles which had been irradiated in increasing increments of 50 r by the NBS.

The phosphate glass needles were mounted in three lucite slides and two masonite sections for insertion in the phantoms (Figure 2.10). Approximately 14 shielded needles were used in each slide with about 36 more imbedded in each of the two special masonite sections. An additional 36 needles were imbedded in each of the four masonite segments of the rack assembly.

2.2.4 Masonite Phantoms. The phantoms are constructed of laminated pressed wood sections of approximately unit density. The phantoms consisted of 20 sections, each 1½ inches thick, to give a total torso height of 30 inches (Figure 2.1). Each phantom was supported by a wooden platform about 30 inches high. The front-to-back thickness of the phantoms was 9 inches (23 cm) and the shoulder width was 18 inches (46 cm). The phantoms were designed so that plastic slides and masonite sections containing the phosphate glass needles could be inserted into the phantoms at various angles and at various elevations from the ground (Figure 2.11). The DT-60/PD's and the IM-107/PD's were mounted on the surface of the phantoms as described in Sections 2.2.1 and 2.2.2. The ratemeter phantom was equipped to hold one sample each of ratemeter types AN/PDR-43 (XN-1) and AN/PDR-44 (XN-1) and one standard depth-dose ratemeter with its detecting element embedded in the phantom at approximately chest height at a depth of 4 cm (Figures 2.2 and 2.12).

2.2.5 Masonite Rack. In addition to the dosimeter phantom, a masonite rack assembly was used for the exposure of dosimeters and for measurement of the concurrent depth dose. The rack was used for all shots for which dosimeter exposures were made with the exception of Shot Priscilla.

The rack assembly consisted of four masonite slabs each measuring 36 inches long, 8 inches wide, and 4½ inches high. The slabs were mounted on a wood frame so that the undersurfaces of the individual slabs were 1, 2, 3, and 4 feet off the ground (Figure 2.13). The individual slabs were identified as Rack I, Rack II, Rack III, and Rack IV, the numerical designation being indicative of the height of the particular slab above the ground.

The masonite slabs had a series of holes drilled at a distance of 4 cm from the front and back and to such a depth that the glass-needle dosimeter would be located at the center height of the slab (Figure 2.13). Wood dowels were used to close the holes after insertion of the shielded needles. In this manner, the homogeneity of the rack was preserved as much as possible.

2.2.6 AN/PDR-43 (XN-1). Radiac AN/PDR-43 (XN-1) (Reference 9) is a small, portable, battery-operated (two BA-30 batteries in series) ratemeter manufactured for the Navy by the Electronic Products Company, Mt. Vernon, New York, (Figure 2.14). The instrument is designed to indicate within 20 percent the field intensity of gamma radiation between 0.5 to 500 r/hr in three ranges. Provisions are made for beta indication, and an internal beta source was used for checking instrument operation. The AN/PDR-43 utilizes a pulsed Geiger-Mueller tube as the detecting element. The tube is operated at a direct-current voltage below threshold and is made sensitive to radiation by means of a shaped voltage pulse superimposed on the direct-current voltage. The voltage pulses are obtained from a relaxation oscillator circuit operating at a pulse repetition rate of approximately 1,400 cps. The Geiger-Mueller (G-M) tube is sensitive to radiation only for the duration of each voltage pulse. The duration of each pulse is small compared to the dead-time of the tube, so that the tube can produce no more than one count during each applied oscillator voltage pulse. This mode of operation permits

Figure 2.8 Reader for phosphate-glass needles.

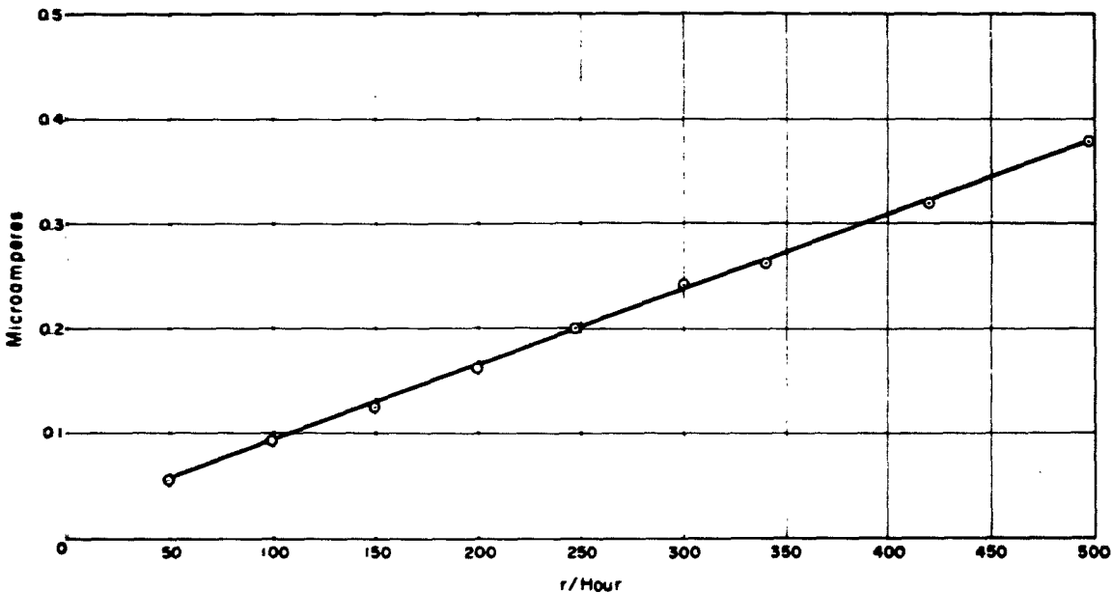

Figure 2.9 Calibration curve for phosphate-glass needles and reader, Co^{60}.

extending the useful range of the G-M tube from the mr/hr region to the r/hr region. The number of G-M tube pulses produced, is proportional to the probability of an ionizing event occurring within the tube during the time the fixed, pulsed, overvoltage is applied (on-time). The G-M tube pulse rate is therefore a measure of the radiation field. Range changing is effected by changing the width of the on-time 1,400-cps pulse. Thus, the least range (0 to 5 r/hr) has

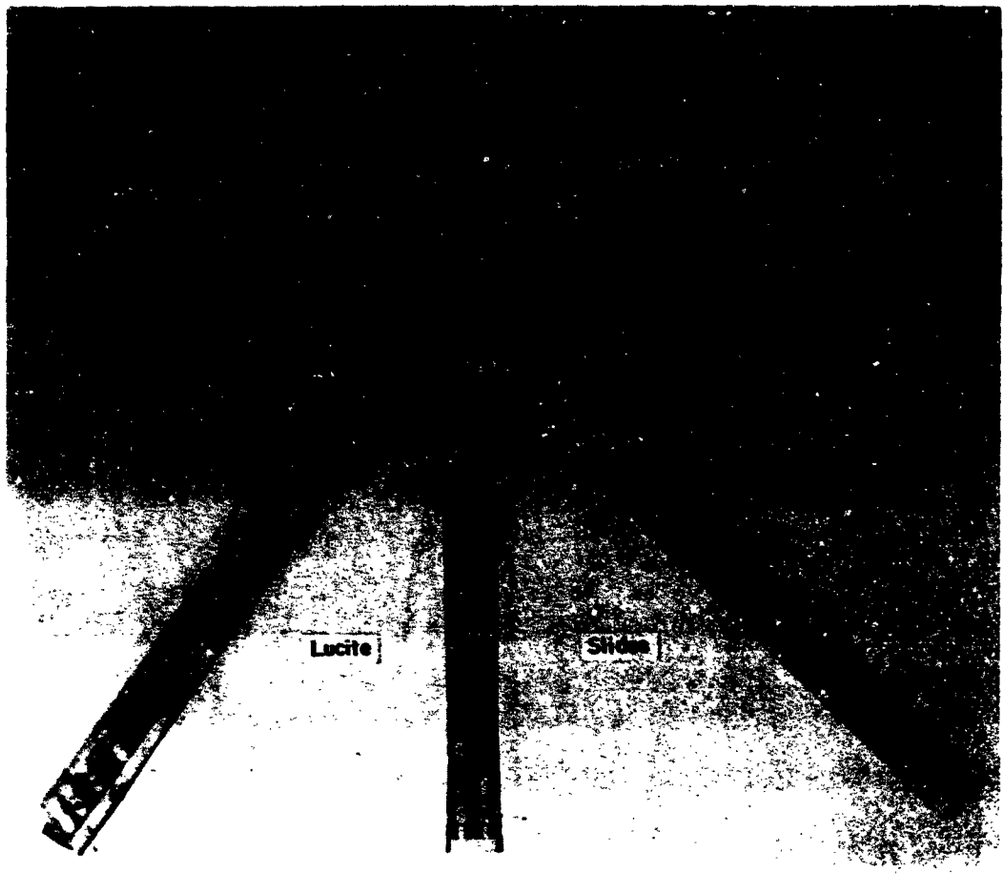

Figure 2.10 Slides and sections loaded with phosphate-glass needles for insertion in masonite phantoms.

the greatest pulse width to compensate for the reduced probability of an ionizing event occurring in a field of this intensity. The instrument is designed to give an air-equivalent response within 20 percent for gamma energies in the range, 80 kev to 1.25 Mev.

2.2.7 AN PDR-44 (XN-1). Radiac set AN/PDR-44 (XN-1) (Reference 10) is a portable, battery-operated (one BA-30 battery) ratemeter, designed by the Naval Radiological Defense Laboratory (NRDL) and manufactured for the Navy by the Admiral Corporation, Chicago (Figure 2.14). The instrument utilizes a pressurized gamma-sensitive ionization chamber for indicating gamma radiation in one of three ranges: 0 to 5, 0 to 50, and 0 to 500 r/hr. Readings were displayed over a 20-ma. linearly marked scale, equipped with a mechanical range-

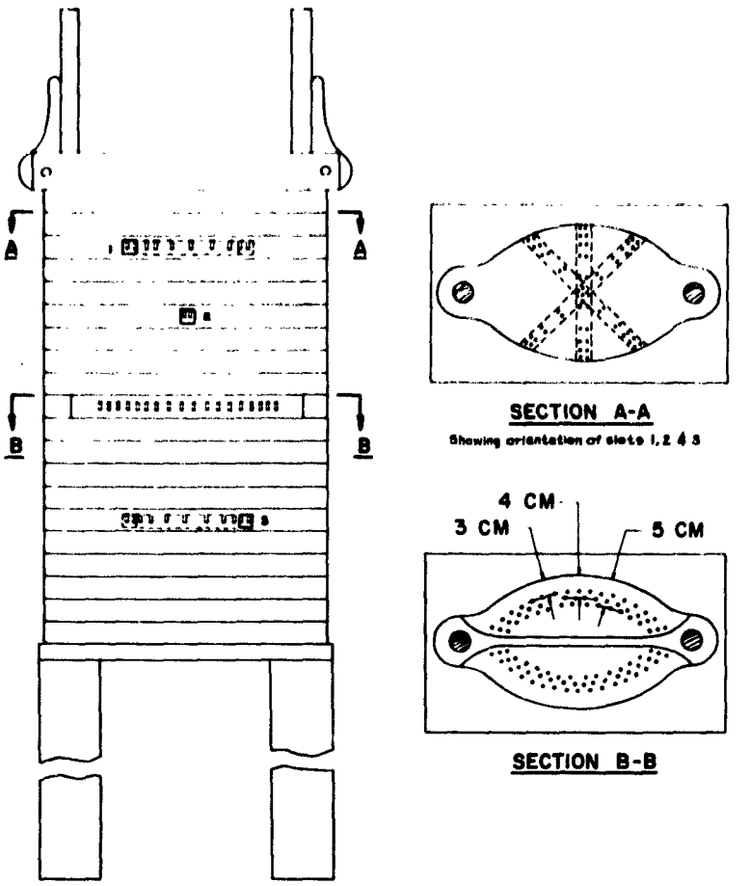

Figure 2.11 Diagram showing location of slides and sections in masonite phantoms.

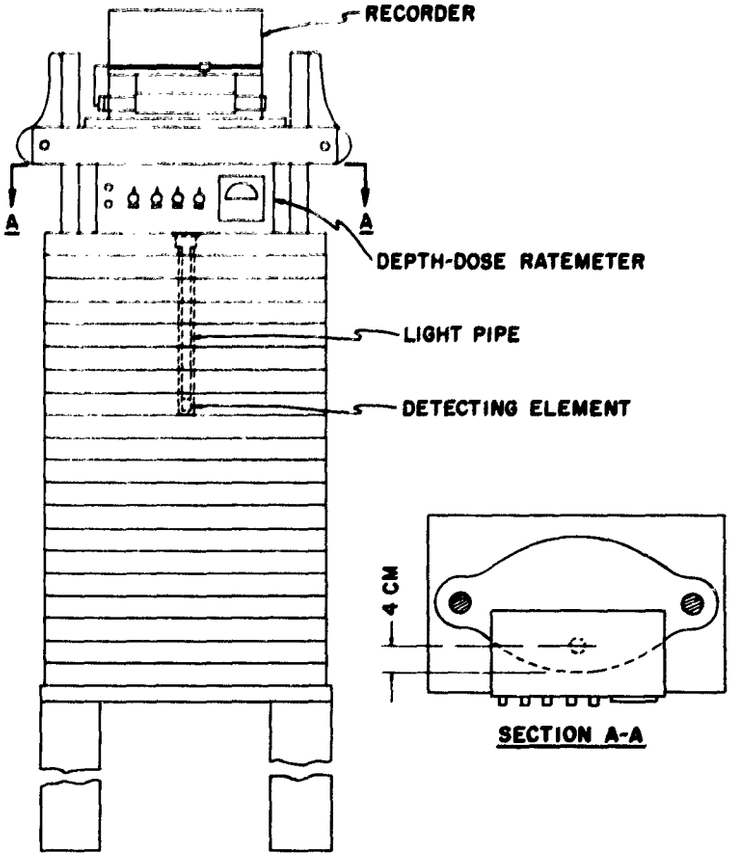

Figure 2.12 Diagram of masonite phantom equipped with depth-dose ratemeter, showing location of detecting element and light pipe.

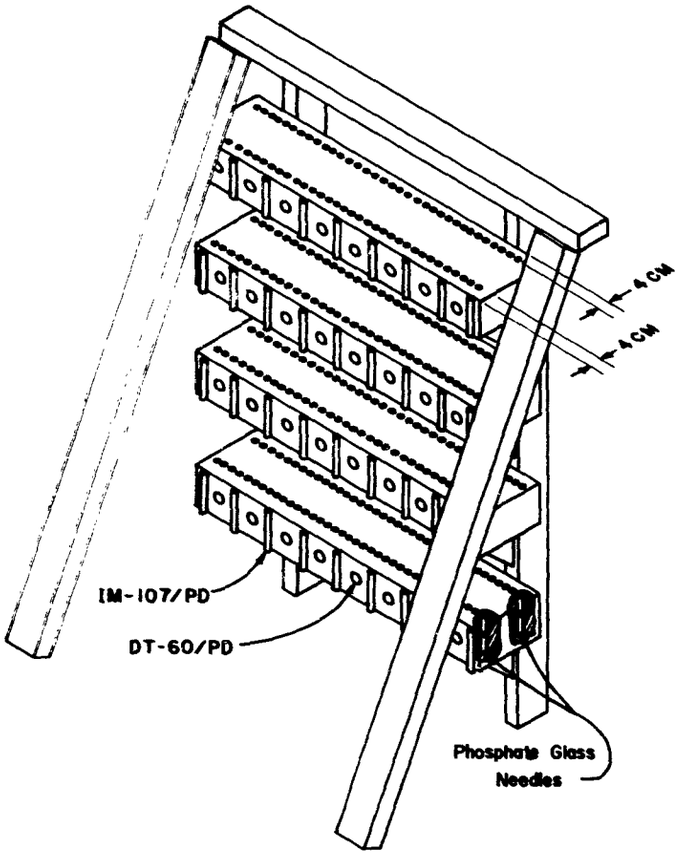

Figure 2.13 Diagram of rack showing location of surface dosimeters and shielded needles.

Figure 2.14 Photograph of standard depth-dose ratemeter and ratemeter Types AN/PDR-43 (XN-1) and AN/PDR-44 (XN-1).

changing system. The meter is driven by a computer-indicator circuit consisting of a stable differential amplifier type of electrometer vacuum-tube volt meter (VTVM) circuit using a dual-tetrode electrometer tube. The reading accuracy of the instrument between 10 and 100 percent of full scale is ± 20 percent for gamma radiation in the energy range 80 kev to 1.25 Mev.

2.2.8 Depth-Dose Ratemeter. A depth dose ratemeter (Figure 2.14) was utilized in this operation as the standard against which the two ratemeter types under investigation (AN/PDR-43 (XN-1) and AN/PDR-44 (XN-1)) were compared. The depth-dose ratemeter had its detecting element imbedded in the phantom at a depth of 4 cm at approximately chest height, and the dose rate obtained at this point was recorded and compared with the recorded readings obtained for the above phantom-held ratemeters. The detecting element for the standard ratemeter is a scintillon plastic phosphor 1 cm in diameter and 1 cm high. A strip of zinc-sulfide (silver activated) 2 mm wide was wrapped around the periphery of the phosphor at midheight to correct the energy dependence of the bare scintillon phosphor. A lucite light pipe, 1 cm in diameter and approximately 12 inches long, was used to transmit the phosphor response to a LP21 photomultiplier tube located at the top of the phantom (Figure 2.12). The density of the lucite is 1.18 gm/cm^3, and it is considered that the lucite-phosphor combination does not alter the tissue equivalence of the phantom. The photomultiplier tube output was read directly on a 100-mv Varian Associates recorder.

The response of the instrument with the detecting element imbedded in the phantom (depth 4 cm) was compared to the air-equivalent response of a Victoreen ratemeter (similarly imbedded) for gamma radiation (70 kev to 1.25 Mev) incident on the surface of the phantom. The results are shown in Figure 2.15. The indicated accuracy of the instrument is within 10 percent for energies between 40 kev and 1.25 Mev and within 5 percent for a Co^{60} air dose.

The range of the instrument is 20 r/hr, with readings indicated linearly on 5-inch recorder paper, allowing a reading accuracy of 0.1 r/hr. The zero shift of the instrument was found to be negligible for repeated 20-hour runs. The response of the phantom imbedded instrument for Co^{60} exposures in 2-r/hr steps up to 20 r/hr is shown in Figure 2.16.

The 4-cm-depth-dose ratemeter recording may be integrated over the exposure time and the resultant dose compared with that recorded by the 4-cm needles that sustained the same exposure.

2.2.9 Ratemeter Recording System. Because of the high fields required, the readings of all ratemeters used were recorded for later interpretation. A Varian Associates G-10, 100-mv recorder (with 5-inch chart) was used. To facilitate recording the readings of the three instruments on one recorder, a sampling system composed of motor-driven, cam-actuated microswitches was used. This provided a cyclic reading of each ratemeter for approximately 18 seconds each minute. Provision was also made for a 5-second recorder zero check once each cycle. The recorder and sampling system required 110-volt, 60-cycle power, which was supplied by means of six 12-volt storage batteries and a 230-watt inverter. Six paralleled storage batteries were adequate to power the entire recording system for periods in excess of 54 hours, which was the maximum recording time required (Figure 2.4).

2.3 DATA REQUIRED

2.3.1 Laboratory Data. Prior to the actual field work, external shields of various materials, such as stainless steel, duraluminum, lead, and lucite were tested in an effort to correct the response of dosimeter types IM-107/PD and DT-60/PD (while reading a surface dose) to agree with the response of the standard dosimeters (silver phosphate glass needles) imbedded at depths of 4 cm in a masonite phantom. Dosimeter readings were obtained with various shields

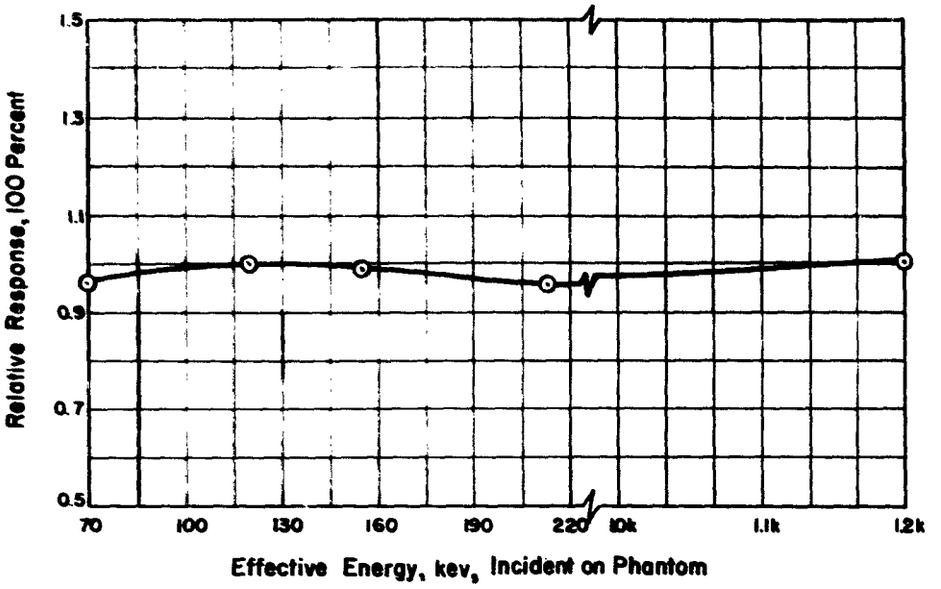

Figure 2.15 Energy dependence curve of ratemeter with detecting element embedded in phantom.

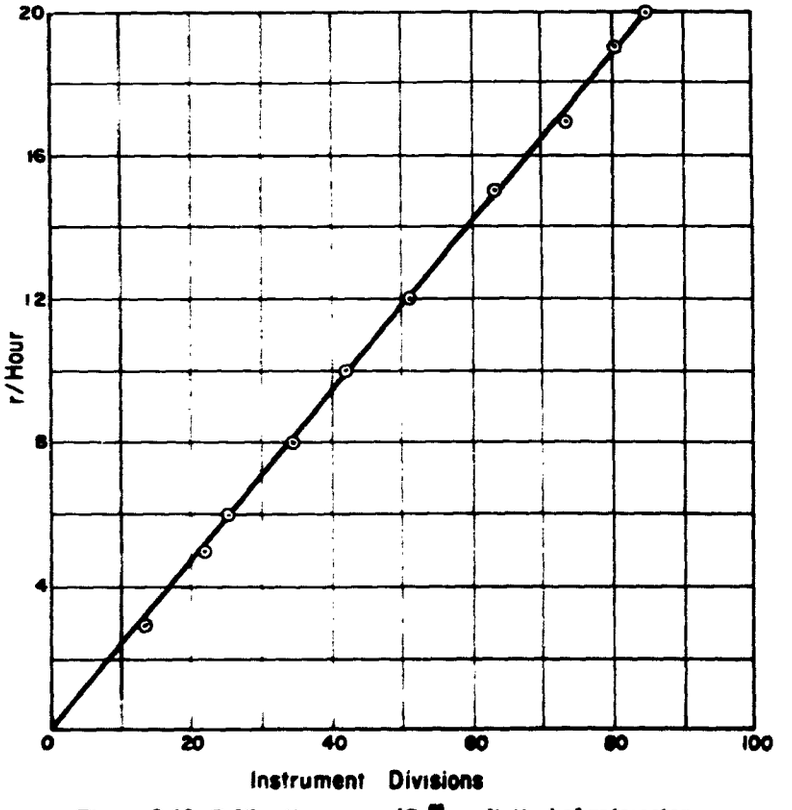

Figure 2.16 Calibration curve (Co^{60} radiation) of ratemeter.

and compared with the readings of the phosphate glass needles for bilateral radiation of energies in the range of 70 kev to 1.25 Mev incident on the phantom. From this data the most effective shields were determined to be 0.06 inch of stainless steel for the IM-107/PD, and 0.012 inch of lead for the DT-60/PD.

2.3.2 Field Data. In the field, the masonite phantoms and sections were loaded with the surface dosimeters, IM-107/PD and DT-60/PD (some selectivity shielded), and with the phosphate glass needles as previously described. Following each exposure the surface dosimeters and the needles were removed from the field and read. Due to nature of the response of the silver phosphate glass to irradiation, the DT-60/PD's and needles were read after a stabilization period of 24 hours. The accuracies of the needles and DT-60/PD dosimeters are considered to be within 20 percent. The accuracy of the IM-107/PD's (preselected as described in Section 2.2.2) is considered to be within 10 percent.

Readings of ratemeter Types AN/PDR-43 (XN-1) and AN/PDR-44 (XN-1) were recorded while the ratemeters were undergoing exposure in residual fields. The recorded readings were compared with the readings obtained with the standard depth-dose ratemeter, which had its detecting element imbedded in the phantom as described in Section 2.2.8. The AN/PDR-43 (XN-1) and AN/PDR-44 (XN-1) ratemeters have a specified accuracy of ± 20 percent for gamma radiation in the energy range of 80 kev to 1.25 Mev. The depth-dose ratemeter had a measured accuracy of within 10 percent for gamma radiation in the energy range 40 kev to 1.25 Mev and within 5 percent for a Co^{60} air dose. The recording system has a rated accuracy of 1 percent and produced no detectable distortion of the response of the three ratemeter types involved.

The estimated accuracy of the field readings contained in the results is of the order of ± 20 percent for both the dosimeter and the ratemeter readings.

Chapter 3
RESULTS

3.1 DESIGN OF SHIELDS

Because of the erroneously high readings of both DT-60/PD's and IM-107/PD's reported from Operation Redwing (Reference 2), shields were designed to bring the response of these detectors as close as possible to the response of the standard phosphate glass needles imbedded to a 4-cm depth in a masonite phantom.

As noted in Section 2.3.1, the optimum shield thickness selected were 0.06 inch of stainless steel for the IM-107/PD dosimeter (1.65 grams/cm^2) and 0.012 inch of lead for the DT-60/PD dosimeter (0.346 grams/cm^2).

Figure 3.1 shows the ratios of the response of the shielded and unshielded IM-107/PD to that of the 4-cm needle for various energies. Figure 3.2 similarly shows the ratios of the shielded and unshielded DT-60/PD. Values in each case are determined from the averages of ten detector readings.

Figures 3.3 and 3.4 show the response of both shielded and unshielded IM-107/PD's and DT-60/PD's, respectively, to the air dose for various energies.

Tables 3.1 and 3.2 present the actual laboratory data obtained in this experiment. No single thickness of shielding was found to bring the ratios in Figures 3.1 through 3.4 to unity for all energies from 80 kev to that of Co^{60}. The shields chosen in both cases tend to reduce response to low-energy (less than 100 kev) radiation to relatively low values. The indicated thicknesses of shielding were chosen, however, based on the criteria that (1) shielding must be thick enough to prevent passage of betas of energies up to several million electron volts, (2) a relatively minor percentage of the dose is contributed by gamma energies below 100 kev, particularly in neutron-induced fields, and (3) doses delivered at energies less than 100 kev is less significant biologically.

The laboratory evaluation was performed with bilateral radiation in all cases. The IM-107/PD's and DT-60/PD's (some selectively shielded) were mounted on the chest of a masonite phantom (Section 2.2.4). The shielded needles were imbedded 4-cm deep in the chest and the phantom was irradiated for a prescribed time. The phantom was then rotated 180 degrees, so the back was now in the position the chest had occupied. An identical exposure was made and a correction factor applied to compensate for the increased distance from the source of the needles and surface detectors. The phantom was removed and the air dose measured, using a Victoreen r-meter placed at the position of the phantom's chest. As described in Sections 2.2.1 and 2.2.2, dosimeters used in this experiment had previously been selected from a group found to be accurate within 5 percent when tested with a radium point source.

3.2 CHARACTERISTICS OF SHIELDED DOSIMETERS

Figure 3.1 shows that the shielded IM-107/PD's read slightly lower than the 4-cm needle dose for the entire energy range between 80 kev and that of Co^{60} (1.25 Mev) with relative response very close to unity at higher energies. At Co^{60} energies, the shielded DT-60/PD's read 1.17 times the 4-cm needle reading (Figure 3.2). Thus, if energies encountered during Operation Plumbbob had been approximately those of Co^{60}, the shielded DT-60/PD could be expected to read about 17 percent higher than the shielded IM-107/PD. Similarly, the laboratory data

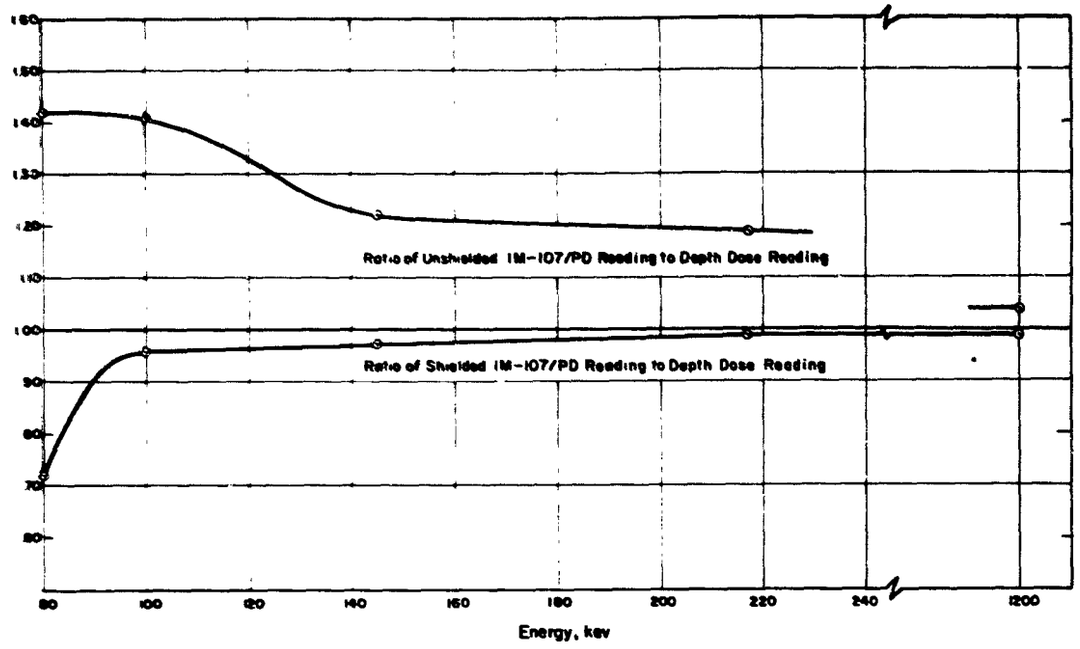

Figure 3.1 Ratios of shielded and unshielded IM-107/PD readings to depth-dose readings.

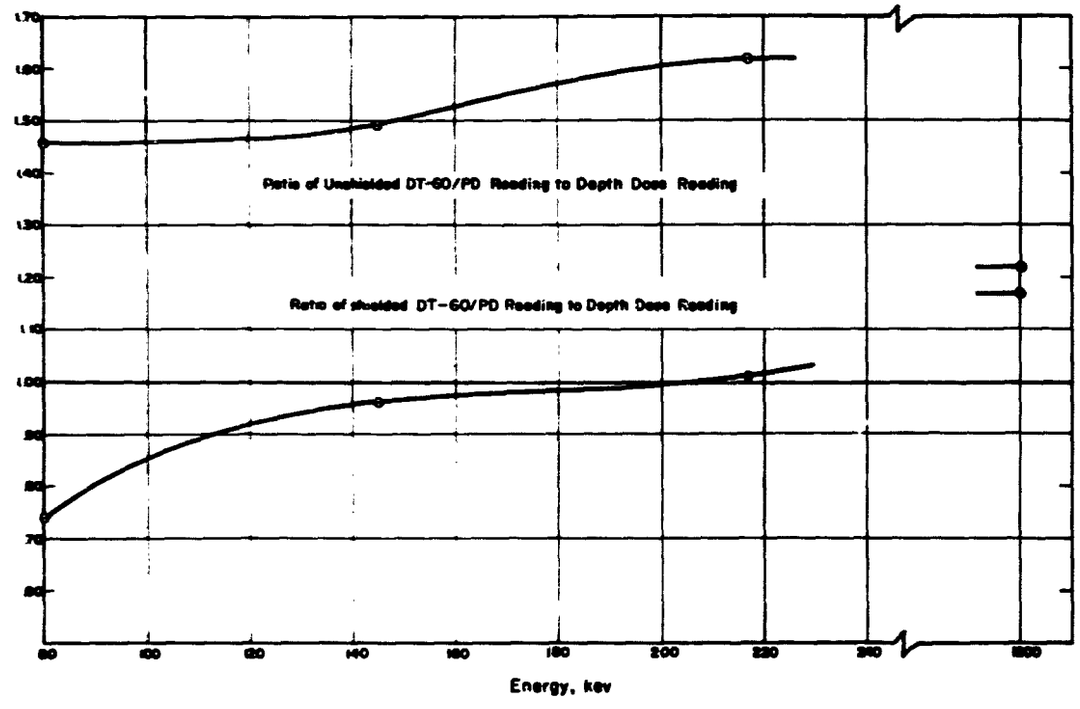

Figure 3.2 Ratios of shielded and unshielded DT-60/PD readings to depth-dose readings.

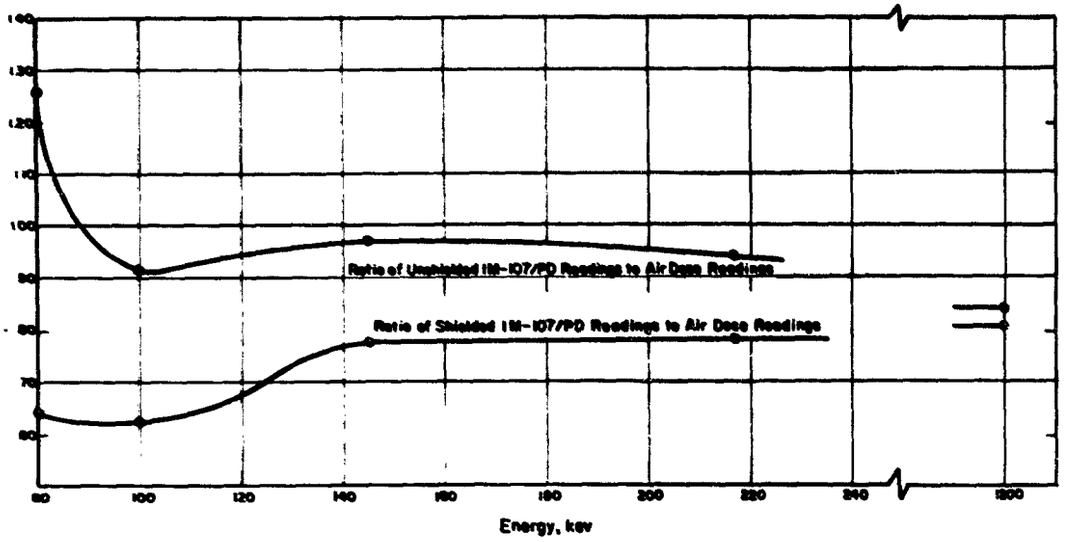

Figure 3.3 Ratios of shielded and unshielded IM-107/PD readings to air-dose readings.

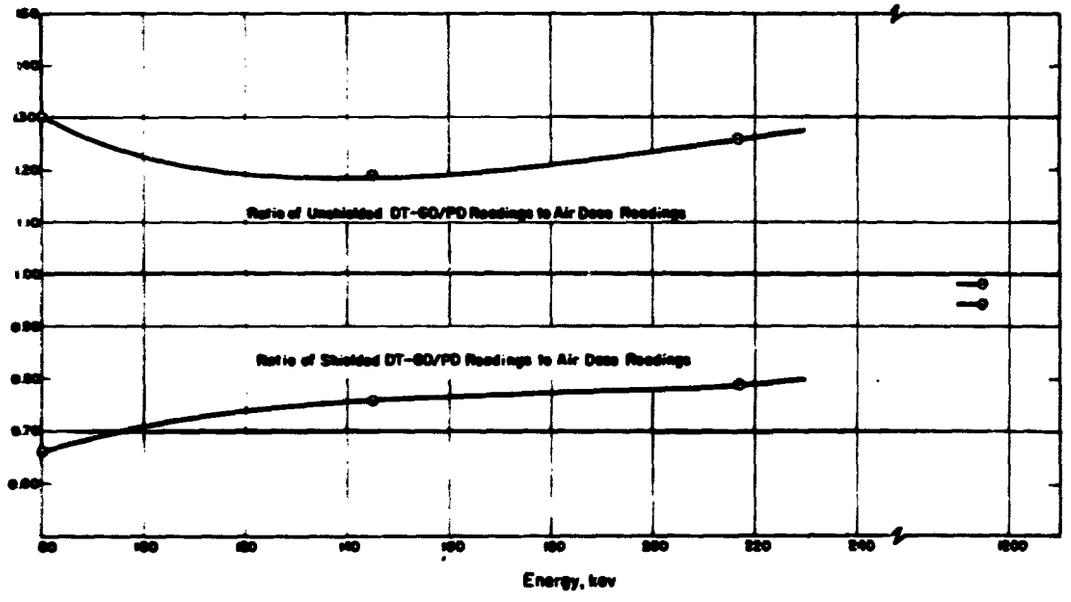

Figure 3.4 Ratios of shielded and unshielded DT-60/PD readings to air-dose readings.

showed that unshielded DT-60/PD's read 22 percent higher than the depth dose values and 17.6 percent higher than the unshielded IM-107/PD values.

3.3 DOSIMETERS

The dosimeter phantoms and rack assembly were displayed during Shots Wilson, Hood, and Diablo. During Shot Priscilla a single dosimeter phantom was used. The tables and figures

TABLE 3.1 AVERAGE DOSES OF SHIELDED AND UNSHIELDED IM-107/PD DOSIMETERS AND 4-CM EMBEDDED NEEDLES

Gamma energy, kev		1,200	217	145	100	80
Distributed air dose-rate*, r/hr		27	188	64	34	16
Average surface reading, ten IM-107/PD dosimeters unshielded, r		22.7	177	62.3	31.1	20.2
Average surface reading, ten IM-107/PD dosimeters shielded with 0.06-inch steel, r		21.7	147.0	49.5	21.2	10.2
Average reading 10 needles, embedded at depth 4 cm, r		21.8	148	51.2	22.0	14.2
Ratio surface to depth-dose readings	IM-107/PD Unshielded	1.04	1.19	1.22	1.41	1.42
	IM-107/PD Shielded with 0.06-inch steel	0.99	0.99	0.97	0.96	0.72

* Bilateral radiation measured with Victoreen r-meter.

giving the data obtained during these exposures are presented according to dosimeter type in the succeeding sections. Tables are used to show the average shielded and unshielded dosimeter dose values. For each type instrument, the average value of all the instruments included on an array is presented, since the variation between individual instruments was purely random. No significance was found in a study of the dosimeter values as a function of height or position on the phantom. This situation of independence of dose value with regard to location on the

TABLE 3.2 AVERAGE DOSES OF SHIELDED AND UNSHIELDED DT-60/PD'S AND 4-CM EMBEDDED NEEDLES

Gamma energy, kev		1,200	217	145	80
Distributed air dose-rate*, r/hr		27	188	64	16
Average surface reading, ten DT-60/PD dosimeters unshielded, r		26.7	239.5	76.2	20.8
Average surface reading, ten DT-60/PD dosimeters shielded with 0.012-inch Pb, r		25.6	149.7	48.9	10.5
Average reading, 10 needles, embedded at depth of 4 cm, r		21.8	148.0	51.2	14.2
Ratio surface to depth-dose readings	DT-60/PD Unshielded	1.22	1.62	1.49	1.46
	DT-60/PD Shielded with 0.012-inch Pb	1.17	1.01	0.96	0.74

* Bilateral radiation measured with Victoreen r-meter.

phantom was true for the three induced-field shots. For Shot Diablo, however, a distinct difference was found between the readings of the front-side and back-side dosimeters. For this reason, average front and back readings are presented for this shot.

Figure 3.5 shows a typical dosimeter array for a phantom with the readings recorded indicated at the dosimeter position. This array was that of the front side of Phantom B in Shot

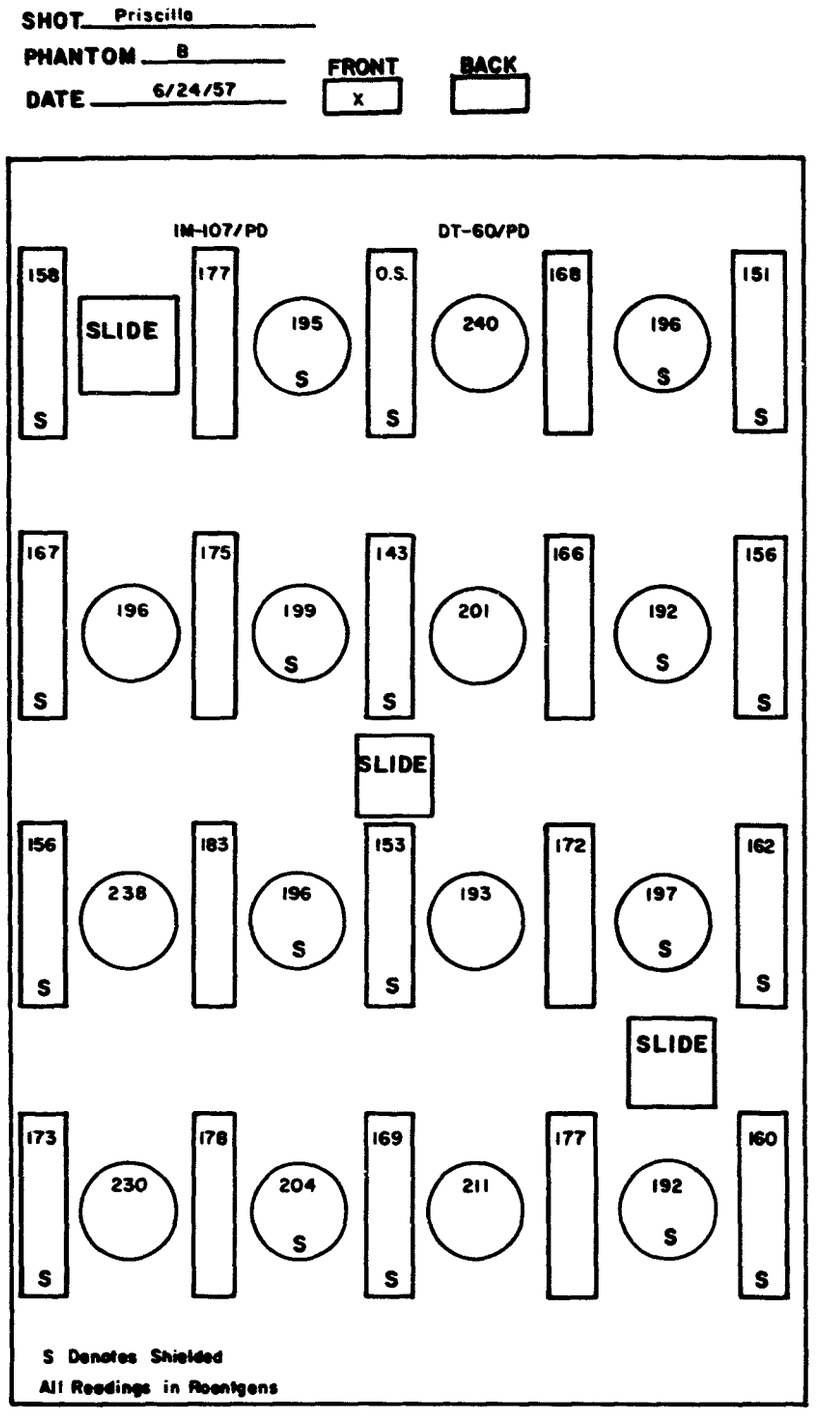

Figure 3.5 Typical phantom dosimeter array.

Priscilla, and the randomness of the readings can be noted. The array is typical of those used for all shots, and the number of shielded and unshielded dosimeters was identical to that illustrated for all phantom exposures. Figure 3.6 illustrates one of the masonite rack sections (Rack I, Shot Hood). Again, the DT-60/PD, IM-107/PD, and needle array are identical to that of all other racks used.

3.3.1 IM-107/PD. The data obtained as the result of the IM-107/PD exposures is presented in Tables 3.3 and 3.4. On Shot Wilson both the shielded and unshielded dosimeters were inadvertently overexposed, and for this reason no data was obtained. The Priscilla participation did, however, produce valid data. As indicated by Table 3.3, the shielded IM-107/PD's were

TABLE 3.3 READINGS OF IM-107/PD'S EXPOSED ON PHANTOMS

Front (F) and back (B) surface detector readings were averaged except for Diablo.

Shot	Phantom Number	IM-107/PD Average Shielded	IM-107/PD Average Unshielded	Average Reading of Needles Embedded at Depth of 4 cm	Ratio of Surface to Depth Dose Readings		Average Ratio of Surface to Depth Readings	
					IM-107/PD Shielded	IM-107/PD Unshielded	Shielded	Unshielded
		r	r	r				
Wilson	A	OS*	OS*	574	—	—	—	—
	B	OS*	OS*	614	—	—	—	—
Priscilla	B	184	168	145	1.06	1.16	1.06	1.16
Hood	A	49	54	53	0.92	1.02	1.01	1.07
	B	53	55	49	1.10	1.12		
		F B	F B	F B	F B	F B		
Diablo	A	102 134	127 163	102 116	1.0 1.16	1.25 1.41	1.05	1.30
	B	90 80	120 160	80 84	1.1 0.96	1.25 1.19		

* OS = Off scale.

6 percent higher than the 4-cm needles, whereas the unshielded instruments read higher than the depth dose needles by 16 percent. The same general situation is observed in the Shot Hood results, for which Tables 3.3 and 3.4 show that the shielded IM-107/PD's average agreed with the depth dose needle readings to within 0.5 percent and the unshielded readings were 6.5 percent higher. Because of the fallout nature of Shot Diablo, the data obtained for the shielded and unshielded dosimeters was quite different. The shielded dosimeter dose was similar to that observed on other shots in that it was 5.5 percent higher than the concurrently exposed 4-cm needles, however, the unshielded values exceeded those of the 4-cm needles by an average of 38 percent.

The results show that the IM-107/PD, when shielded with 0.06 inch of stainless steel, gives readings that agree with the needle depth dose to within 6 percent for both neutron-induced and fallout fields. The unshielded dosimeter data indicates that the readings are between 6 and 16 percent higher than the measured 4-cm needle dose for neutron-induced fields; however, for fallout fields the difference becomes large (30 to 46 percent).

3.3.2 DT-60/PD. The exposure data for the DT-60/PD is presented in Tables 3.5 and 3.6. The DT-60/PD's exposed to Shot Wilson were subjected to a total dose in excess of the 600-r range of the CP-95/PD reader. In order to interpret the indications of these overexposed

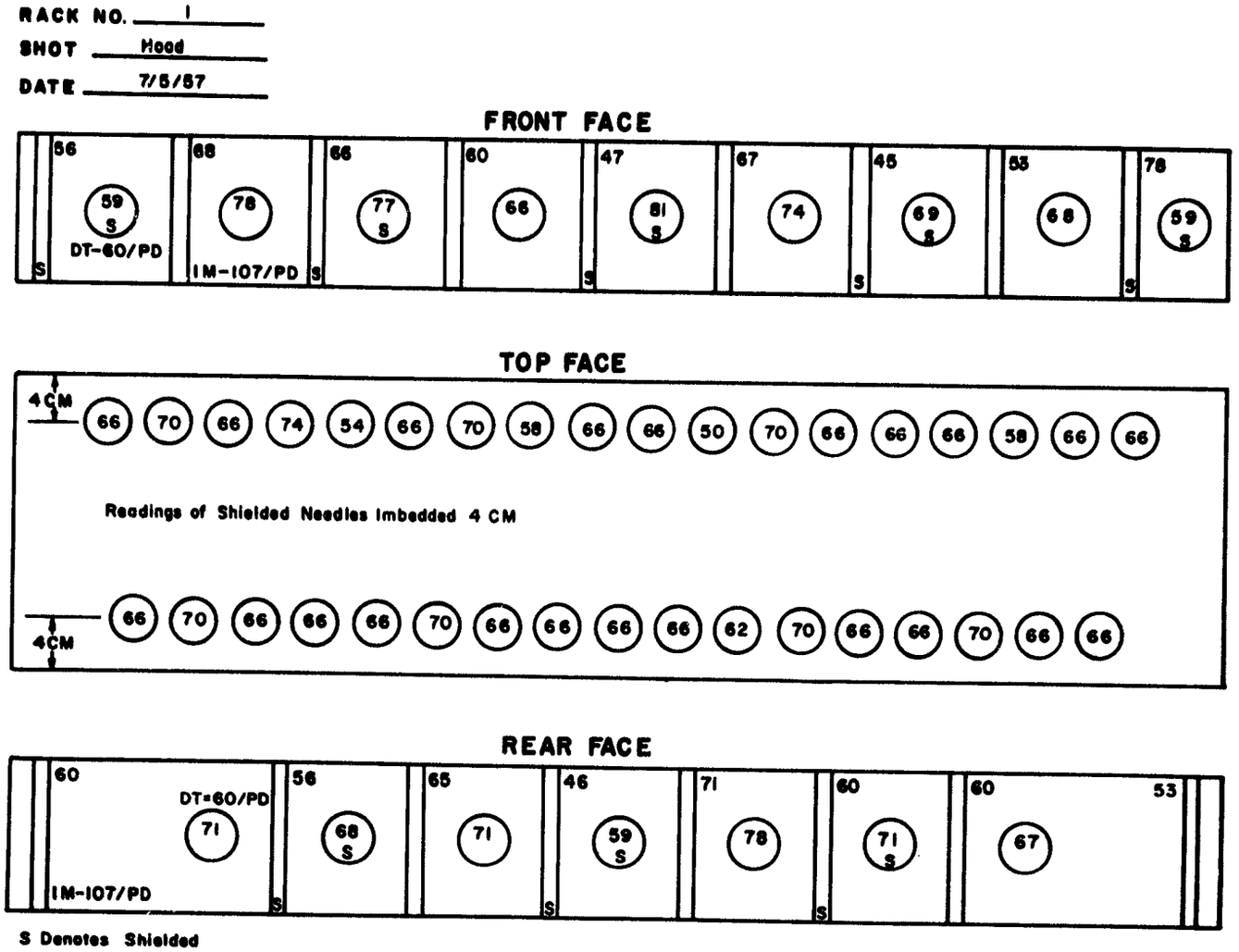

Figure 3.6 Typical rack dosimeter array.

TABLE 3.4 READINGS OF IM-107/PD'S EXPOSED ON RACKS

Front (F) and back (B) surface detector readings were averaged except for Diablo.

Shot	Rack Number	IM-107/PD Average Shielded	IM-107/PD Average Unshielded	Average Reading of Needles Embedded at Depth of 4 cm	Ratio of Surface to Depth Dose Readings IM-107/PD Shielded	Ratio of Surface to Depth Dose Readings IM-107/PD Unshielded	Average Ratio of Surface to Depth Readings Shielded	Average Ratio of Surface to Depth Readings Unshielded
		r	r	r				
Wilson	I	OS*	OS*	730	—	—	—	—
	II	OS*	OS*	687	—	—	—	—
	III	OS*	OS*	678	—	—	—	—
	IV	OS*	OS*	670	—	—	—	—
Hood	I	56	63	60	0.93	1.05		
	II	54	55	52	1.05	1.08	0.98	1.06
	III	53	58	53	0.99	1.09		
	IV	51	55	54	0.95	1.02		
		F B	F B	F B	F B	F B		
Diablo	I	126 129	191 172	114 119	1.11 1.08	1.68 1.45		
	II	133 111	188 164	116 119	1.15 0.93	1.62 1.38	1.06	1.46
	III	126 110	165 147	112 114	1.13 0.97	1.47 1.29		
	IV	128 113	162 155	112 116	1.14 0.97	1.45 1.34		

* OS = Off scale.

TABLE 3.5 READINGS OF DT-60/PD'S EXPOSED ON PHANTOMS

Front (F) and Back (B) surface detector readings were averaged except for Diablo.

Shot	Phantom Number	DT-60/PD Average Shielded	DT-60/PD Average Unshielded	Average Reading of Needles Embedded at Depth of 4 cm	Ratio of Surface to Depth Dose Readings DT-60/PD Shielded	Ratio of Surface to Depth Dose Readings DT-60/PD Unshielded	Average Ratio of Surface to Depth Readings Shielded	Average Ratio of Surface to Depth Readings Unshielded
		r	r	r				
Wilson	A	788	878	574	1.37	1.53	1.34	1.49
	B	806	891	614	1.31	1.45		
Priscilla	B	188	207	145	1.30	1.43	1.30	1.43
Hood	A	64	76	53	1.21	1.44	1.25	1.44
	B	63	71	49	1.29	1.45		
		F B	F B	F B	F B	F B		
Diablo	A	135 156	162 195	102 116	1.32 1.34	1.59 1.68	1.31	1.61
	B	112 112	147 128	89 84	1.23 1.33	1.65 1.52		

DT-60/PD's, several were subjected to accurate doses of 600, 800, and 1,000 r in the laboratory. The CP-95/PD and DT-60/PD system was then calibrated, and the Wilson DT-60/PD's were read. The data obtained from Shot Wilson shows that the shielded detectors read an average of 29 percent higher than the 4-cm needles, whereas the unshielded exceeded the needle dose by 40 percent. The unshielded dosimeter doses exceeded the shielded instrument values by 8.5 percent. For Shot Priscilla it was found that the shielded detectors read an average of 30 percent higher than the 4-cm needles, whereas those unshielded exceeded the needle dose by 43 percent. For Shot Hood it was found that on the average, the shielded DT-60/PD's read 23.5 percent higher than the 4-cm needles and the unshielded versions exceeded the depth dose

TABLE 3.6 READINGS OF DT-60/PD'S EXPOSED ON RACKS

Front (F) and back (B) surface detector readings were averaged except for Diablo.

Shot	Rack Number	DT-60/PD Average Shielded		DT-60/PD Average Unshielded		Average Reading of Needles Embedded at Depth of 4 cm		Ratio of Surface to Depth Dose Readings DT-60/PD Shielded		Ratio of Surface to Depth Dose Readings DT-60/PD Unshielded		Average Ratio of Surface to Depth Readings Shielded	Average Ratio of Surface to Depth Readings Unshielded
		r		r		r							
Wilson	I	916		965		730		1.25		1.32			
	II	839		945		687		1.22		1.37		1.24	1.32
	III	821		869		678		1.21		1.28			
	IV	842		865		670		1.26		1.29			
Hood	I	68		72		60		1.13		1.20			
	II	68		76		52		1.31		1.45		1.22	1.37
	III	66		75		53		1.24		1.42			
	IV	64		77		54		1.19		1.43			
		F	B	F	B	F	B	F	B	F	B		
Diablo	I	140	161	175	191	114	119	1.23	1.35	1.54	1.61		
	II	131	146	173	194	116	119	1.13	1.23	1.49	1.63	1.27	1.61
	III	151	138	181	182	112	114	1.35	1.21	1.62	1.60		
	IV	150	153	194	197	112	116	1.34	1.32	1.73	1.70		

by an average of 40.5 percent. The different nature of the Diablo field is also indicated from the DT-60/PD data obtained for this shot. Whereas the shielded instruments indicated doses higher than the depth dose by an average of 29 percent, the unshielded dosimeters averaged 61 percent higher.

In summary, the DT-60/PD dosimeter, where shielded with 0.12 inch of lead, read doses from 22 to 34 percent higher than the silver phosphate glass needles buried inside a masonite phantom and rack at a depth of 4 cm. This was not an unexpected result, since laboratory data indicated that the shielded DT-60/PD read 17 percent higher than the imbedded needles when irradiated by Co^{60}.

The unshielded detector data again shows considerably greater variance with the 4-cm needle data, as expected. The variation here ranged between 32 and 49 percent for the induced fields and 61 percent for the Diablo field.

3.3.3 Needle Dose Data and Depth Dose Curves. The amount of internal dose sustained as

measured with the silver phosphate needles and its variation as a function of depth within the phantom is shown in Figures 3.7 through 3.13.

The phantom data points indicated on these figures represent the average of the readings of twelve needles for depths of 3, 4, 5, 18, 20, and 21 cm. All other values are the average of six needles. Each individual needle was read three times; however, since the agreement be-

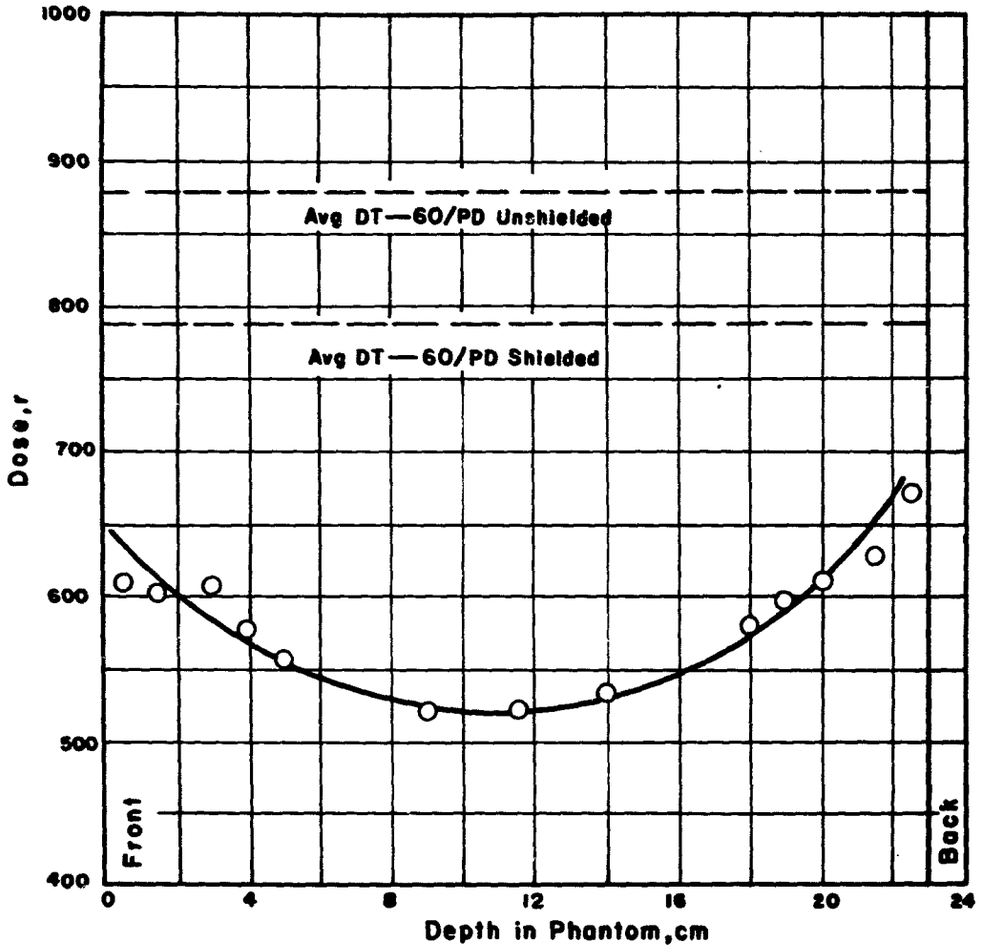

Figure 3.7 Shot Wilson, Phantom A, dose as a function of depth.

tween readings was very close, it was not necessary to average the values. A typical set of needle dose data is shown in Table 3.7. This table shows the corrected average needle reading in microamperes (predose subtracted) and the resultant dose in roentgens. It depicts the needle situation for Phantom B, Shot Priscilla, and is typical of all the 4-cm needles. Smooth curves were fitted visually to the data points to prepare the previously referenced figures.

As indicated previously, two phantoms and one rack were utilized for all shots except Priscilla. For this shot, only one dosimeter phantom was used. Since it was necessary to provide some separation between the rack and phantoms upon their installation in the field, the

individual units were subjected to slightly different fields and, therefore, sustained somewhat different total doses. This fact is evident in the different total doses recorded by the needles contained in the two phantoms and four rack sections for the same total exposure period.

The actual measured doses as indicated by the 4-cm needles were used in the preparation

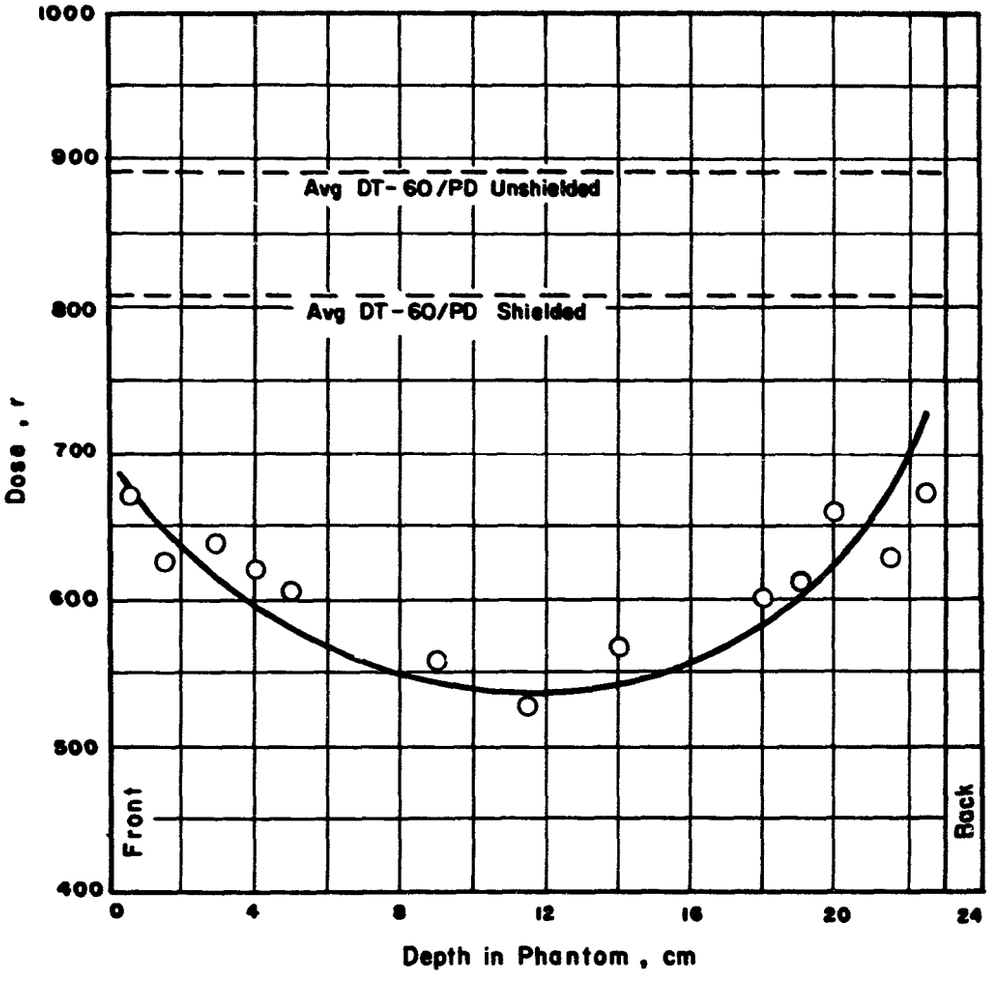

Figure 3.8 Shot Wilson, Phantom B, dose as a function of depth.

of Tables 3.3 to 3.6, in which the readings of the DT-60/PD and IM-107/PD dosimeters are compared.

In the preparation of Table 3.8, which shows the relation of the midline dose to the 4-cm dose for the phantoms, the midline dose was estimated from the curves of Figures 3.7 to 3.13. It is evident from the data presented in this table that the midline dose is about 10 percent lower than the 4-cm dose for induced fields. For an unperturbed fallout field, such as the one to which the forward side of Phantom B and the back side of Phantom A were subjected during Shot Diablo, a much-greater variance was noted between the 4-cm and midline doses. This, of course, is a

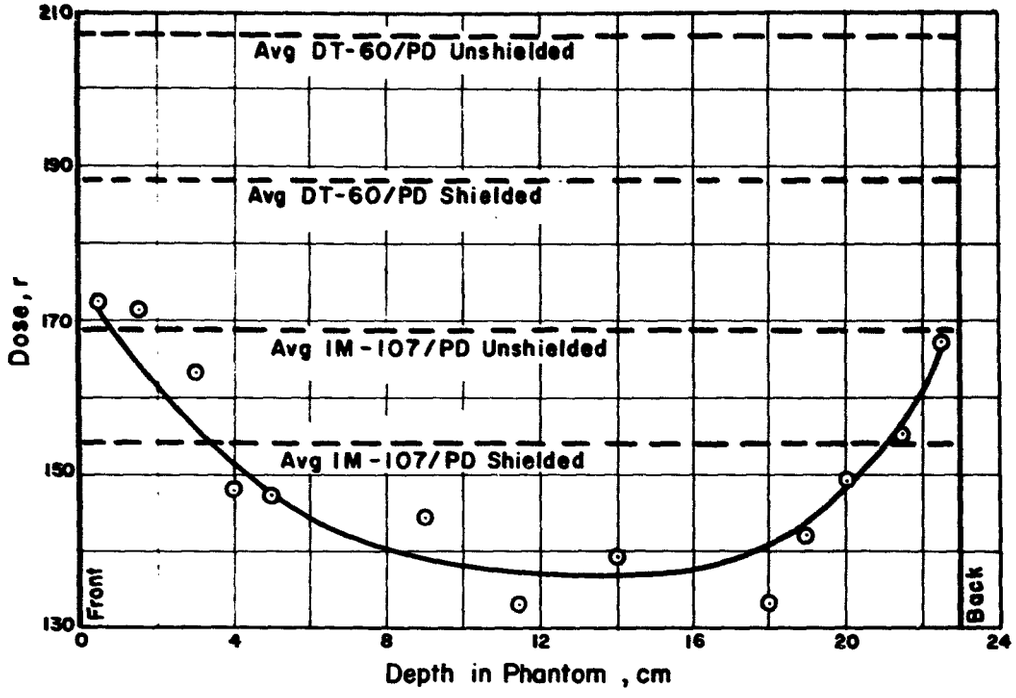

Figure 3.9 Shot Priscilla, Phantom B, curve of dose as a function of depth.

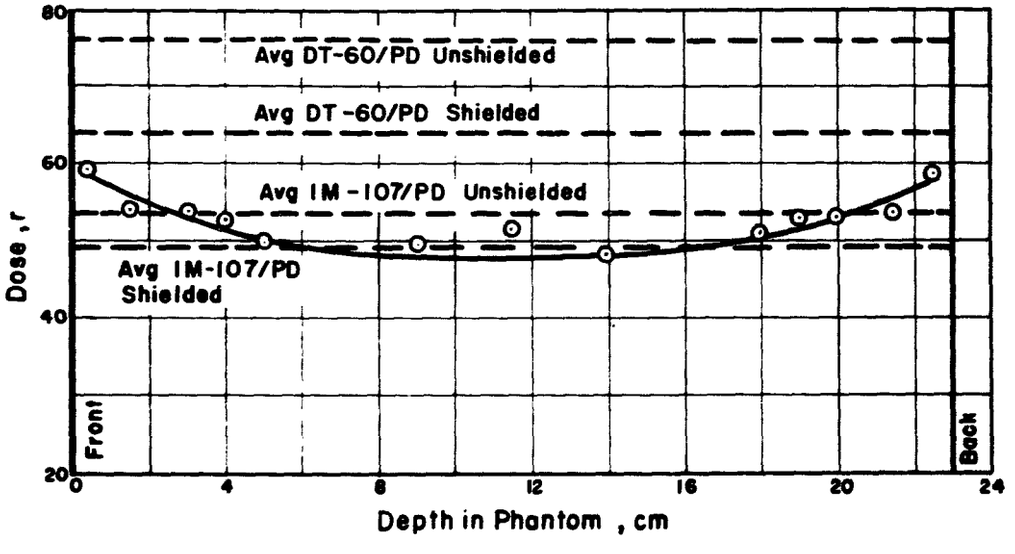

Figure 3.10 Shot Hood, Phantom A, curve of dose as a function of depth.

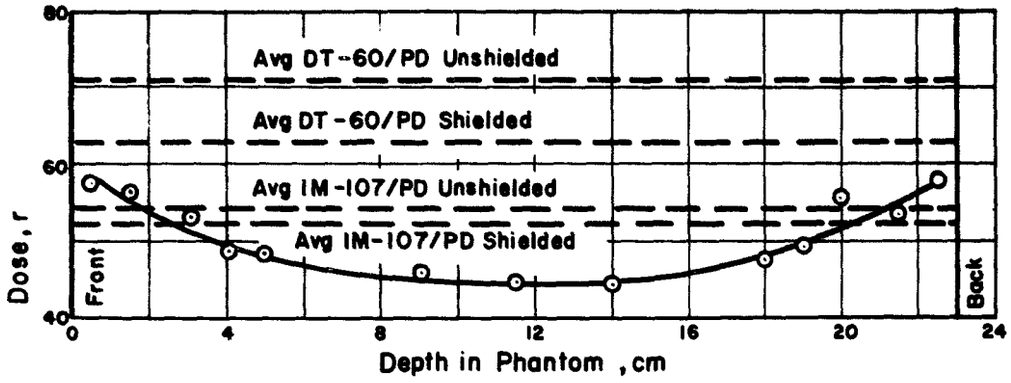

Figure 3.11 Shot Hood, Phantom B, curve of dose as a function of depth.

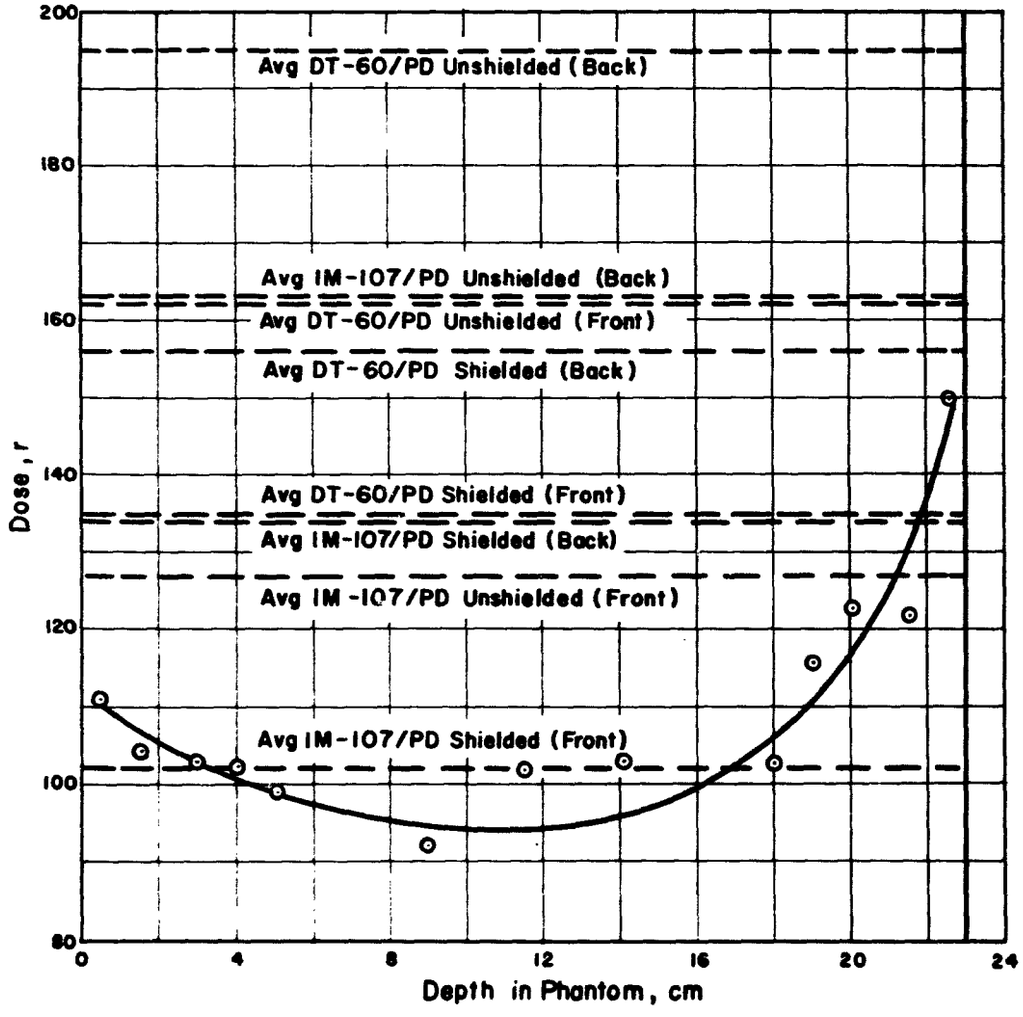

Figure 3.12 Shot Diablo, Phantom A, curve of dose as a function of depth.

consequence of the lower-energy characteristic of the fallout field. As was previously noted, the Diablo field was definitely asymmetric with respect to the phantom being exposed. There was a steep gradient between the road and a location just off the road where the phantoms were placed. In addition, the stalled truck served to further perturb the field. For these reasons,

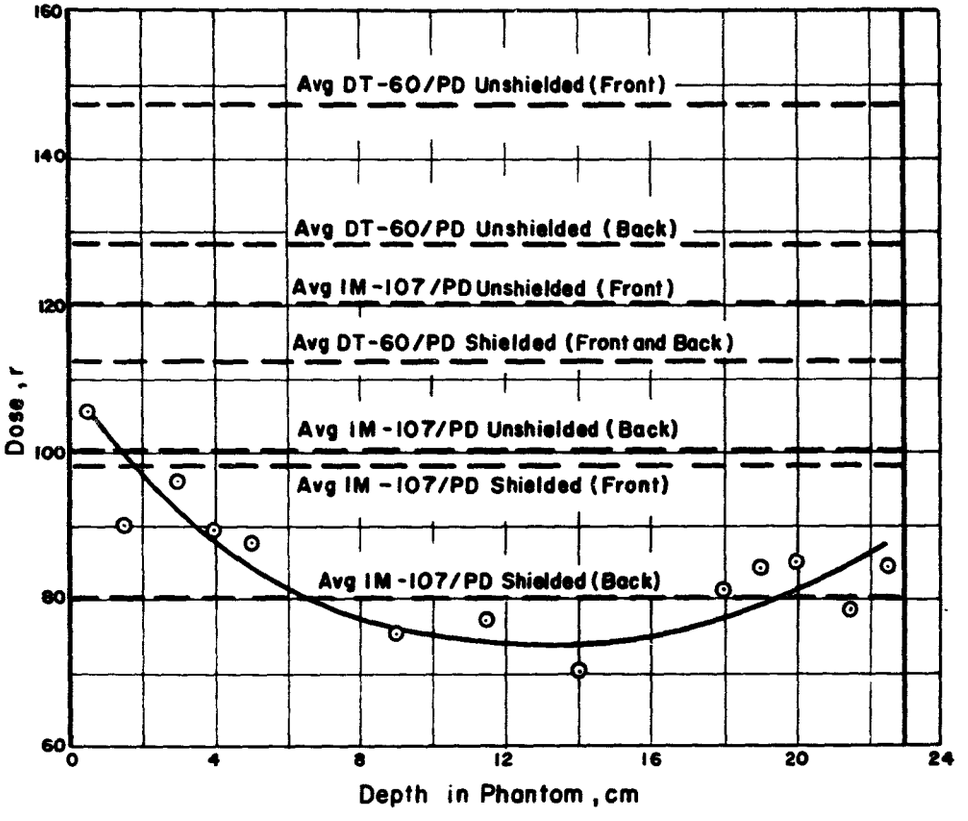

Figure 3.13 Shot Diablo, Phantom B, dose as a function of depth.

the comparison of the 4-cm needle dose with the midline dose for the sides away from ground zero is considered to be nonrepresentative of a uniform-fallout-field situation.

3.4 RATEMETER

The ratemeter phantom was exposed to Shots Wilson, Priscilla, Hood, and Diablo. The recorded dose rates as a function of time, which were obtained from the exposures on the first three shots, are presented graphically in Figures 3.14 through 3.16. Since only AN/PDR-44 data was obtained from Wilson, a single record is presented in Figure 3.14. For Shots Priscilla and Hood, the corresponding figure presents dose rate versus time for the AN/PDR-43 (XN-1), the AN/PDR-44 (XN-1), and for the depth-dose ratemeter. The Diablo data is not presented for reasons explained later in the report.

The curves for measured dose rate versus time are presented as solid lines on the figures; however, the curves have been extrapolated mathematically. The extrapolated portion of the

TABLE 3.7 GLASS NEEDLE DATA FOR FIGURE 3.9, PHANTOM B, SHOT PRISCILLA*

Dose is obtained by subtracting average predose value for the inherent fluorescence of the needles (24.5×10^{-3} microamp) and then dividing the corrected average reading in microamperes by a calibration constant (75×10^{-5}) which is the slope of the calibration curve of microamperes versus roentgens (Figure 2.9), which has the dimensions of microamperes per roentgen.

Depth From Front	Corrected Average Reading	Dose
cm	μa	r
0.5	0.1305	174
1.5	0.130	173
3.0	0.122	163
4.0	0.111	148
5.0	0.110	147
9.0	0.108	144
11.5	0.100	133
14.0	0.104	139
18.0	0.100	133
19.0	0.1065	142
20.0	0.112	149
21.5	0.116	155
22.5	1.25	167

* This data is typical of all events.

TABLE 3.8 PERCENT OF 4-CM DEPTH DOSE REPRESENTED BY MIDLINE (11.5 CM) DOSE

In Diablo, Phantoms A and B faced oppositely.

Phantom	Shot	Midline (11.5 cm) Dose	Average of Front And Back 4-cm Dose		Difference of 4-cm Dose	
		r	r		pct	
A	Wilson	517	574		9.9	
B	Wilson	535	614		12.9	
A	Hood	48	51.5		6.9	
B	Hood	44.5	49.7		10.5	
B	Priscilla	138	148		6.8	
			Front	Back	Front	Back
A	Diablo	94	101	111	7.0	14.5
B	Diablo	74	88	79	16.0	6.4

curves is shown by dashed lines. The method by which this extrapolation was performed is discussed fully later in this report. The purpose of this extrapolation was to permit comparison of the total doses as recorded for a known period of time by the dosimeters (DT-60/PD, IM-107/PD, and 4-cm needles) and that obtained by integrating the dose rate values over the same time period.

To facilitate the presentation of the ratemeter results, the data pertaining to all three ratemeter types will be presented according to the shot in which the data was obtained.

3.4.1 Shot Wilson. As in the case of the DT-60/PD's and IM-107/PD's for this shot, no data was obtained for the AN/PDR-43 (XN-1) and the depth-dose ratemeter. The high radiation field

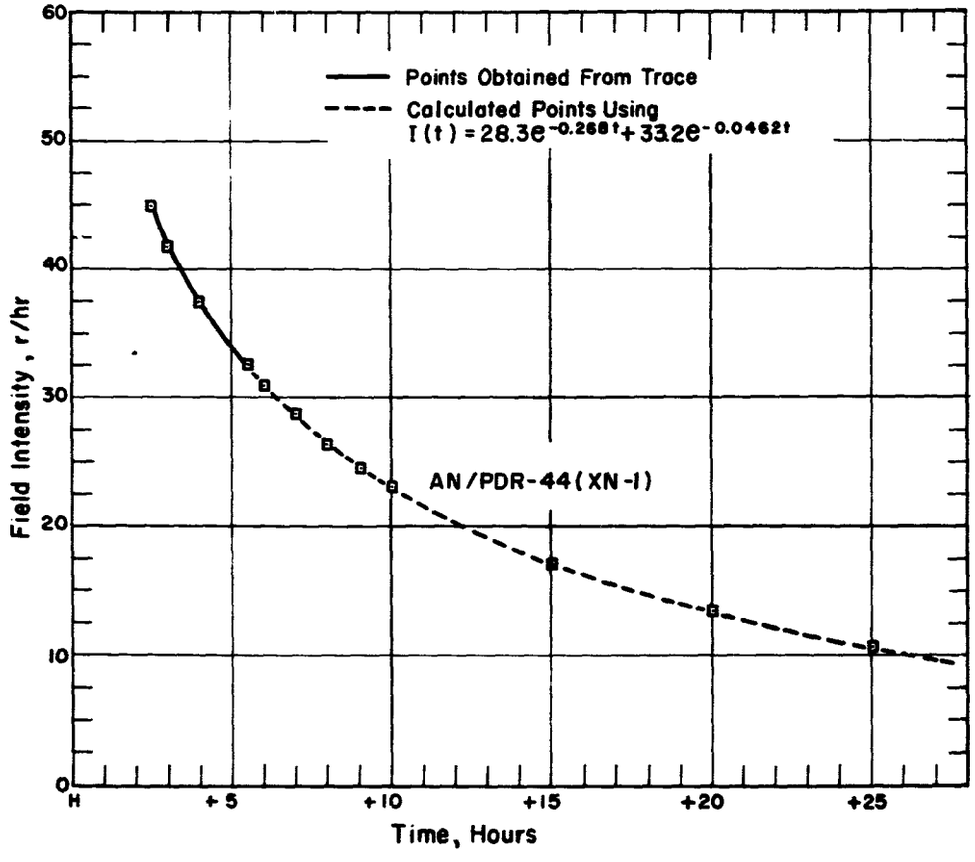

Figure 3.14 Shot Wilson, decay of AN/PDR-44 (XN-1).

in which the phantom was located produced dose rates exceeding the maximum dose-rate capability of the recorder for the entire period of operation (6 hours). For the AN/PDR-43 (XN-1) this was 15.6 r/hr; the limiting maximum value for the depth-dose ratemeter was 23.4 r/hr.

The AN/PDR-44 recorder had a maximum rate capability of 45 r/hr, and data was obtained for a period of 3 hours. The measured values as a function of time are presented by the solid line in Figure 3.14. As previously mentioned, the measured curve has been extrapolated mathematically and is noted by the dashed-line portion of this figure.

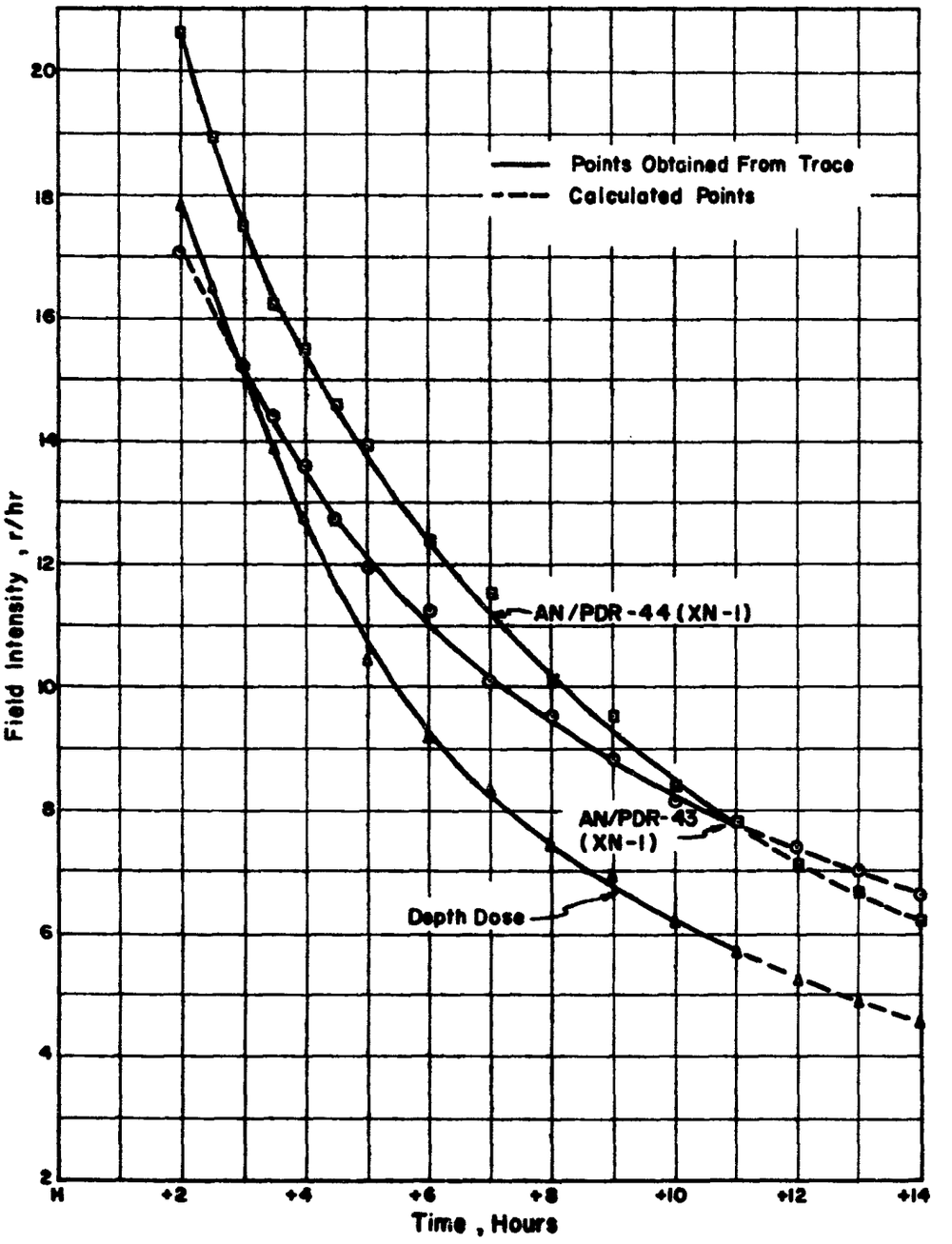

Figure 3.15 Decay of AN/PDR-44 (XN-1), AN/PDR-43 (XN-1), and depth-dose ratemeter, Shot Priscilla. Depth dose $I(t) = 16.1e^{-0.35t} + 7.91e^{-0.046t}$, AN/PDR-43 (XN-1) $I(t) = 11.0e^{-0.35t} + 11.7e^{-0.046t}$, AN/PDR-44 (XN-1) $I(t) = 17.9e^{-0.35t} + 11.1e^{-0.046t}$.

3.4.2 Shot Priscilla. During Shot Priscilla, data was obtained for all three instrument types. In the case of the AN/PDR-44 (XN-1) and depth-dose ratemeter, the measured data extends from the time of exposure (H + 2 hours) until H + 11.5 hours, when the recorder unit failed. The field intensity exceeded the maximum dose-rate capability of the AN/PDR-43 recorder for the first hour after exposure. The AN/PDR-43 (XN-1) trace did not come on scale until H + 3 hours, and recorded properly until H + 11.5 hours. The recorded traces for all three instruments are given

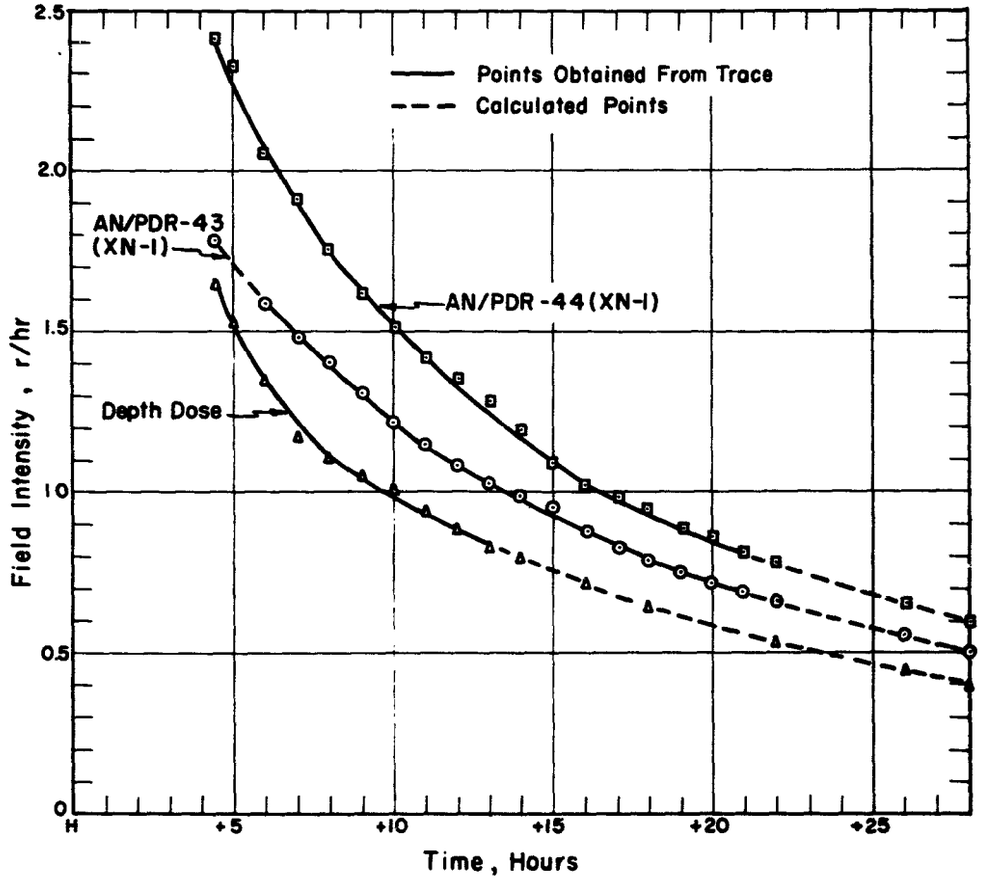

Figure 3.16 Decay of AN/PDR-44 (XN-1), AN/PDR-43 (XN-1), and depth-dose ratemeter, Shot Hood. Depth dose $I(t) = 1.45e^{-0.28st} + 1.43e^{-0.046t}$, AN/PDR-43 (XN-1) $I(t) = 0.97e^{-0.28st} + 1.82e^{-0.046t}$, AN/PDR-44 (XN-1) $I(t) = 1.94e^{-0.28st} + 2.14e^{-0.046t}$.

in Figure 3.15. In this figure, the extrapolation of the AN/PDR-43 (XN-1) data is shown by a dashed line.

Figure 3.17 shows the ratios of the AN/PDR-43 (XN-1) and AN/PDR-44 (XN-1) readings to the depth-dose ratemeter reading as a function of time. The sharp increase in these ratios to about 6 hours is not understood.

3.4.3 Shot Hood. The data obtained for the meters during this participation is shown on

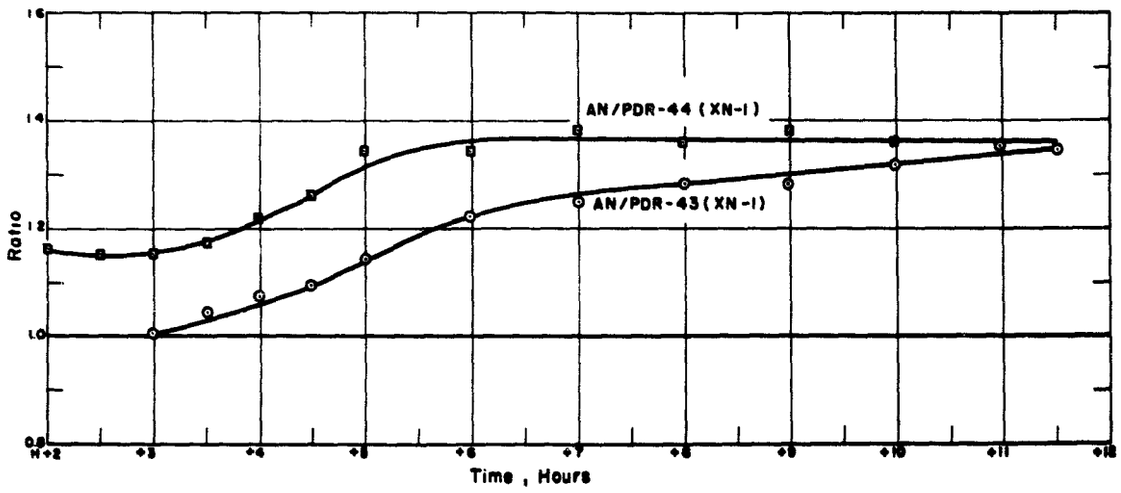

Figure 3.17 Ratios of AN/PDR-43 (XN-1) and AN/PDR-44 (XN-1) to ratemeter, Shot Priscilla.

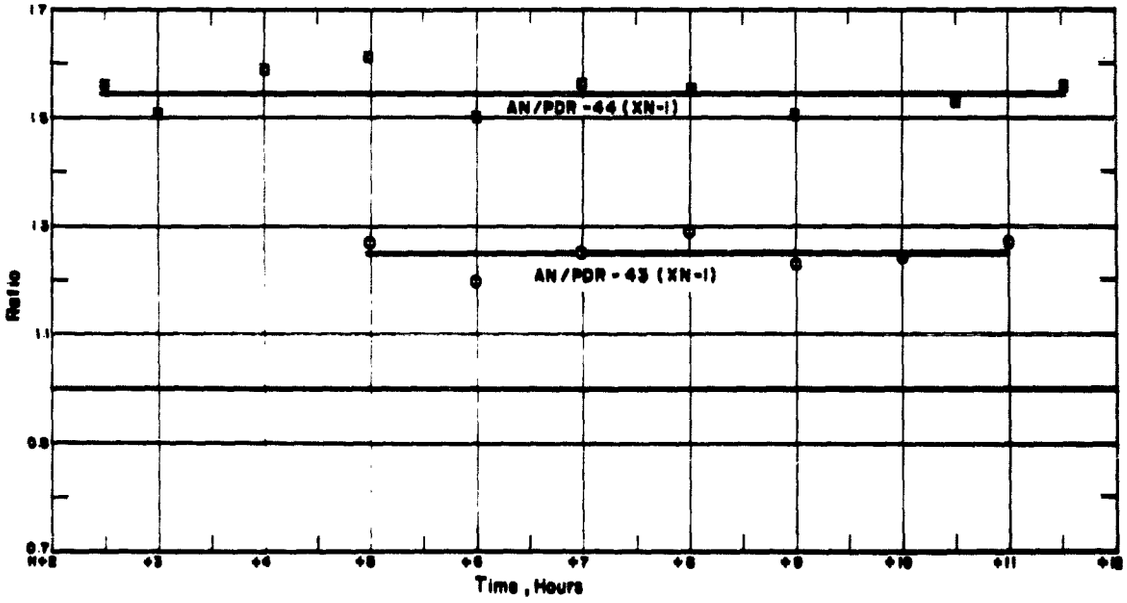

Figure 3.18 Ratios of AN/PDR-43 (XN-1) and AN/PDR-44 (XN-1) to ratemeter, Shot Hood.

Figure 3.16. The AN/PDR-43 (XN-1) capability was again exceeded at early times, and the recorder did not come on scale until H + 6 hours. The trace for the depth-dose ratemeter became indeterminable at H + 13 hours, which was probably due to the fact that the field intensity had decayed to such a point that the meter was reading in the range of 4 percent of full scale. As in the case of the other curves, the measured curves were extrapolated mathematically.

In Figure 3.18 the values of the ratios of AN/PDR-43 (XN-1) and AN/PDR-44 (XN-1) readings to ratemeter readings are shown. Unlike the situation in Shot Priscilla, the ratios are approximately constant, averaging about 1.25 for the AN/PDR-43 (XN-1) and 1.55 for the AN/PDR-44 (XN-1).

3.4.4 Shot Diablo. The data obtained during the Diablo exposure indicated that the calibration of the ratemeter-recorder combination changed in some manner. This was evident from the fact that both the AN/PDR-43 (XN-1) and AN/PDR-44 (XN-1) readings were lower than those for the ratemeter.

After laboratory investigation, it was found that a short circuit had developed in the ratemeter. As a result, the full battery-supply voltage of the ratemeter (900 volts) was impressed across the metering circuit of the other radiacs through the cycling timer. Since the meter movements of the AN/PDR-43 (XN-1) and AN/PDR-44 (XN-1) and the input circuit of the Varian recorder that sampled the radiac meter current were severely damaged, no interpretation of the recorder trace is possible.

Chapter 4
DISCUSSION

4.1 CHARACTERISTICS OF PLUMBBOB RADIATION FIELDS

During initial planning, the project was informed that precautions would be taken during the operation to prevent fallout. Therefore, the project planning was based on the premise that the instrument evaluation would be carried out in neutron-induced fields only. This was not considered entirely satisfactory, as far as this project was concerned, as the results of Redwing (Reference 2) had indicated that beta radiation was probably the primary cause for the high readings of the nonshielded DT-60/PD and IM-107/PD's. Since a neutron-induced field is characterized by high-energy gamma radiation and a small beta component, it did not lend itself to evaluating what was expected to be primarily a beta effect. Under these conditions, the project was planned to obtain data applicable only to neutron-induced soil activity. As it turned out, however, a significant fallout field did result from Shot Diablo, and the evaluation of the instruments in both type fields became possible.

Shots Wilson, Priscilla, and Hood, which were balloon shots, produced typical neutron-induced fields, composed almost entirely of the radiation from Na^{24} ($t_{1/2}$ = 15.0 hr; 1.38 and 2.76 Mev gamma energies), Mn^{56} ($t_{1/2}$ = 2.58 hr; 0.845, 1.81, 2.13 Mev gamma energies) and Al^{28} ($t_{1/2}$ = 2.27 min, 1.78 Mev gamma energies). At the times at which the project instrumentation was displayed, the Al^{28} activity had decayed to insignificant levels and was disregarded. The beta activity of these fields was minimal, and in general there was no indication of a soft component at times later than H + 4.25 hours (Reference 13).

As previously stated, the Diablo field was a pure fallout field. This was a tower shot, and the nuclear device was so shielded that the neutron flux was attenuated by a factor of 1 million. Because of this attenuation, and considering the distance at which the instruments were displayed, the resulting exposures were due only to fallout radiation.

Since the two types of fields are quite different in respect to the energy distribution of the radiations involved, the effects on the dosimeters were expected to be very different. That this was true is apparent from the results previously presented on the individual dosimeters.

4.2 EFFECTIVENESS OF DOSIMETER SHIELDS

4.2.1 IM-107/PD. As indicated by Tables 3.3 and 3.4, the 0.06-inch stainless-steel shielding was effective in reducing the dosimeter indication so that good agreement existed between the shielded IM-107/PD readings and those of the 4-cm glass needles. For both the neutron-induced field and the fallout field the agreement between the shielded IM-107/PD and needle depth dose was within 6 percent. Comparison of the readings of shielded and unshielded dosimeters shows that the shielding reduced the dosimeter response by an average of 8 percent for the induced field; however, for the fallout field the reduction averaged 32 percent. This follows directly from the energy characteristics of the two fields, the fallout field having a relatively larger soft component that was effectively attenuated by the added shielding.

4.2.2 DT-60/PD. The data presented in Tables 3.5 and 3.6, shows that the 0.12-inch lead shielding used on the DT-60/PD did not produce as effective results as the IM-107/PD shield-

ing. The shielded DT-60/PD readings ranged from 22 to 34 percent higher than their 4-cm-needle counterparts. That this should occur was not surprising, since as previously discussed, the laboratory tests of the shields for energies of Co^{60} gave results that were about 17 percent high. The difference between this anticipated excess and that actually observed can also be partially explained. For the DT-60/PD instrument, the roentgen indication increases as a linear function of the temperature (Reference 11) at time of irradiation. The instrument response to 1 r of dose increases by 0.278 percent per degree Fahrenheit increase in temperature. Considering the average temperature of the surface DT-60/PD's as being at least the average NTS daytime temperature (100 F), an increased response of the instrument of the order of 5 percent would be expected.

Comparison of doses recorded by the shielded and unshielded DT-60/PD's indicates that the shielded dosimeter read an average of about 9 percent lower in induced fields and about 20 percent lower in the fallout field. Again this is attributed to the different energy nature of the fields.

A preliminary evaluation of the DT-60/PD results indicates that although the 0.12-inch lead shielding significantly improved the response of the instrument with respect to its measurement of equivalent depth dose, the shield was not yet completely satisfactory. Based on laboratory studies conducted since the field test, it was found that shields selectively reducing the higher-energy response could be designed that would satisfactorily correct the response characteristics of the DT-60/PD dosimeters. This shielding was found to be 0.20 inch of lead with four holes, $^3/_{64}$-inch diameter, symmetrically spaced through each face of the shield.

4.2.3 Comparison of Surface Detectors in Operations Plumbbob and Redwing. It was found in Plumbbob that the unshielded DT-60/PD indicated a higher dose than the unshielded IM-107/PD. This effect is in direct contrast with the parallel observations of the DT-60/PD's and IM-107/PD's above deck in Redwing (Reference 2), but is in concurrence with the effects noted below deck. This effect in Plumbbob is believed to be due to the insignificant effect of beta radiation present in all fields encountered, paralleling the situation existing below decks of ships in Operation Redwing. Since the Diablo field was entirely of a fallout nature, it might have been expected that the results obtained could be likened to the Redwing data for above-deck dosimeters. That this was not the case can be explained by the different procedures used. In Shot Diablo the experimental arrays were placed in the field after the major part of the fallout had settled and were never in close proximity with beta radiating particles. In Operation Redwing the phantoms were situated prior to shot time and were directly subjected to the fallout (see Section 3.1 of Reference 2). The Operation Redwing phantoms were also wrapped in polyethylene sheeting to prevent contamination by the fallout. This sheeting was wrapped about the phantom in a fashion such as to create numerous pockets into which fallout collected. Thus, many dosimeters were in close proximity to beta-emitting fallout debris. Since the heavier-walled DT-60/PD would be less sensitive to this radiation than the IM-107/PD, the reading of the latter was found to be higher. For Operation Plumbbob, polyethylene sleeves were again utilized; however, great care was taken to insure that the sheeting provided a completely smooth surface without pockets. In this way, no trap for settling fallout particles or wind distributed activity was created.

Since the beta dose produced by transient fallout particles during deposition or wind transfer would be small in comparison to the total dose, that for the Diablo instruments was assumed as coming from a plane source field in which an appreciable amount of the beta radiation was attenuated before reaching the dosimeters on the phantoms. Under these circumstances, the normal heavier wall of the DT-60/PD would not be as effective in producing a sharp difference between the reading of this dosimeter and the IM-107/PD.

The data obtained by this project indicates that for situations in which there is no essentially direct contact with fallout debris, the unshielded IM-107/PD gives a lower dose indication than the unshielded DT-60/PD.

4.3 PERFORMANCE OF RATEMETERS

4.3.1 AN/PDR-43 (XN-1). Data was obtained on the performance of the AN/PDR-43 from Shots Priscilla, Hood, and Diablo. Although the instrument was exposed to Shot Wilson, the existing dose rates were beyond the maximum capability (15.6 r/hr) of the ratemeter-recorder combination. The ratio of AN/PDR-43 reading to depth-dose ratemeter as a function of time for Shot Priscilla is shown by Figure 3.17. The ratio increases rather sharply with time until approximately 6 hours and then becomes fairly stable. The corresponding curve for Shot Hood (Figure 3.18) does not show an increase in the ratio for the AN/PDR-43 versus depth-dose ratemeter, the ratio being approximately constant and having an average value of 1.25. The ratemeter readings obtained for Shot Diablo are invalid because of equipment failure.

4.3.2 AN/PDR-44 (XN-1). Usable data on the performance of the AN/PDR-44 (XN-1) was obtained from Shots Wilson, Hood, and Priscilla. As in the case of the AN/PDR-43, the Diablo data is not interpretable due to equipment failure. The situation regarding the curves showing ratios of AN/PDR-44 to ratemeter readings as a function of time is similar to that found for the AN/PDR-43. For Priscilla, an increasing ratio to 6 hours is noted (Figure 3.17), whereas the Hood ratio (Figure 3.18) is fairly constant, maintaining an average value of 1.55.

It is considered that the increasing ratio obtained for Priscilla was due to a change in the AN/PDR-43 calibration during the run. The calibration change was noted prior to the re-use of this instrument during Shot Hood.

4.3.3 Comparison of Integrated-Ratemeter with Dosimeter Doses. To obtain a cross comparison of the accuracy of the dosimeters and ratemeters evaluated in this project, a check of the total dose indicated by the dosimeters against that obtained by integrating the ratemeter values over identical exposure times was performed. The curves obtained from the ratemeter results were extrapolated to encompass the times over which the dosimeter exposures were made. Figures 3.14 (Wilson), 3.15 (Priscilla), and 3.16 (Hood) present these extrapolated curves. The method used in this extrapolation is discussed fully below, as are the techniques used for accomplishing the integrations.

The Wilson residual field was due to induced activity. As discussed in Section 4.1, the primary activities making up the field were Na^{24}, Mn^{56}, and Al^{28}. As the project equipment was installed at H + 45 minutes, the Al^{28} activity was negligible, having decayed through more than fifteen half lives. Assuming then that only Na^{24} and Mn^{56} activities are involved, the equation for the field intensity at any time can be represented as follows:

$$I(t) = I_{\theta_1} e^{-a_1 t} + I_{\theta_2} e^{-a_2 t}$$

Where: I_{θ_1} = initial activity of field contributed by Mn^{56} r/hr

I_{θ_2} = initial activity of field contributed by Na^{24} r/hr

a_1 = disintegration constant for Mn^{56} = 0.268 1/hr

a_2 = disintegration constant for Na^{24} = 0.0462 1/hr

t = hours after zero time

In order to find I_{θ_1} and I_{θ_2}, it is only necessary to know the total intensity of the field at any two times t_1 and t_2. Hence for the Wilson field at 2 hours and 20 minutes after zero time,

$$I(t) = 44.9 \text{ r/hr} = I_{\theta_1} e^{-0.268(2.33)} + I_{\theta_2} e^{-0.0462(2.33)}$$

At 5 hours and 30 minutes after zero time,

$$I(t) = 32.4 \text{ r/hr} = I_{0_1} e^{-0.268(5.5)} + I_{0_2} e^{-0.0462(5.5)}$$

These are two equations with two unknown quantities, I_{0_1} and I_{0_2}. Thus it can be determined that

$$I_{0_1} = 28.3 \text{ r/hr} \quad \text{and} \quad I_{0_2} = 33.2 \text{ r/hr}$$

and the equation for I(t) becomes

$$I(t) = 28.3 e^{-0.268t} + 33.2 e^{-0.0462t}$$

This equation can now be used to extrapolate the curve for measured dose rate versus time to earlier and later times. Since the recorded dose-rate traces did not normally extend to the time when the dosimeter exposures were terminated, nor in some cases did the ratemeter traces come on scale until sometime after an exposure had been started, it was necessary to extrapolate the dose-rate curves to the times of interest.

Utilizing the equation or the extrapolated curves, a mathematical or graphical integration can be performed over the period of time the dosimeter arrays were in the field. For Wilson, this time was from H + 45 minutes to H + 54 hours. Table 4.1 shows the integrated doses for the three types of ratemeter and the 4-cm-needle doses, shielded and unshielded IM-107/PD average doses, and shielded and unshielded DT-60/PD average doses for each phantom and rack exposed. The dose as determined by integration of the AN/PDR-44 readings over the aforementioned interval was 723 r. When this value is compared with the average dose as recorded by the glass needles at 4 cm in the phantoms and racks (Table 4.1), it is noted that the AN/PDR-44 dose averages 9.7 percent higher. When compared with the average dose recorded by the unshielded DT-60/PD's, the AN/PDR-44 dose averages 19.7 percent lower.

For Priscilla, dose rate versus time was recorded by all three instruments to H + 11 hours. As the phantom dosimeters were exposed until H + 54 hours, it was again necessary to extrapolate the curves in order to obtain a comparison of dose values. The derived equations used in accomplishing the extrapolation were as follows:

AN/PDR-43: $I(t) = 11.0 e^{-0.268t} + 11.7 e^{-0.0462t}$

AN/PDR-44: $I(t) = 17.9 e^{-0.268t} + 11.1 e^{-0.0462t}$

Depth Dose Ratemeter: $I(t) = 16.1 e^{-0.268t} + 7.9 e^{-0.0462t}$

In each case the values of the initial activity were calculated from readings taken with the ratemeter for which they were being determined.

Integration of the curves was performed graphically to H + 11 hours and mathematically from H + 11 to H + 54 hours.

For the depth-dose ratemeter the integration of the dose rate over the indicated time period yielded a total dose of 179 r. This is 23 percent greater than the dose recorded by the 4-cm needles (145 r), 16 percent greater than the shielded IM-107/PD's (154 r), and 5 percent less than the shielded DT-60/PD's (188 r).

The integration of the AN/PDR-43 rates yielded a total dose of 234 r, whereas the AN/PDR-44 integration showed a total dose of 240 r. A comparison with the 4-cm dose indicates that the AN/PDR-43 read 61 percent high and the AN/PDR-44 was high by 65 percent. When the AN/

PDR-43 integrated dose is compared with the unshielded IM-107/PD and DT-60/PD doses, values of 39 percent and 13 percent higher, respectively, are noted.

When the AN/PDR-44 integrated dose is compared with the unshielded IM-107/PD and DT-60/PD doses, values of 43 and 16 percent higher, respectively, are noted.

These latter comparisons (unshielded surface detectors to AN/PDR-43 and AN/PDR-44) are considered significant as they compare measurement of a surface dose.

For Shot Hood, dose-rate readings were obtained for the ratemeter to H + 11 hours and for the AN/PDR-43 and AN/PDR-44 to 19 hours. As was previously explained, the ratemeter phantom was inadvertently placed in a lower field than originally intended because of a 10-r/hr reading on the road, which decreased sharply to approximately 2 r/hr in the field alongside. The dosimeter phantoms were immediately moved to a higher field (7 r/hr as indicated by an AN/PDR-43). This procedure could not be followed for the ratemeter phantom, as the recorder power

TABLE 4.1 READINGS OF DETECTORS, EMBEDDED NEEDLES, AND RATEMETERS, IN ROENTGENS

Shot	Phantom and/or Rack	Needles Embedded at 4 cm	DT-60/PD Average		IM-107/PD Average		Depth-Dose Ratemeter Integrated 4 cm Dose	PDR-43 Integrated Air Dose	PDR-44 Integrated Air Dose
			Shielded	Unshielded	Shielded	Unshielded			
Wilson	A	574	788	878	—	—			
	B	614	806	891	—	—			
	I	730	916	965	—	—			
							—	—	723
	II	687	839	945	—	—			
	III	678	821	869	—	—			
	IV	670	842	865	—	—			
Priscilla	B	145	188	207	154	168	179	234	240
Hood	A	53	64	76	49	54			
	B	49	63	71	53	55			
	I	60	68	72	56	63			
							75	102	119
	II	52	68	76	54	55			
	III	53	66	75	53	58			
	IV	54	64	77	51	55			
Diablo	Data not possible								

supply was being shared with another project. Not only was it necessary to extrapolate the curves in order to obtain a comparison of dose values with the dosimeter phantoms, but the integrated doses predicted by the ratemeter had to be scaled up to be equivalent to that which would have been accumulated by the ratemeter in a 7-r/hr field.

The derived equations used in the extrapolation of the curves were:

$$\text{AN/PDR-43:}\quad I(t) = 0.97\,e^{-0.268t} + 1.82\,e^{-0.0462t}$$

$$\text{AN/PDR-44:}\quad I(t) = 1.94\,e^{-0.268t} + 2.14\,e^{-0.0462t}$$

$$\text{Depth Dose Ratemeter:}\quad I(t) = 1.45\,e^{-0.268t} + 1.43\,e^{-0.0462t}$$

Integration was performed graphically up to 11 hours for the depth-dose ratemeter and up to 19 hours for the AN/PDR-43 and -44 and then formally up to 54 hours. The integrated dose values were then scaled up by a factor of 7/2.16, where 2.16 is the calculated initial intensity

of the field (indicated by the AN/PDR-43) in which the ratemeter phantom was placed. Calculation of this value was necessary as full-scale deflection for the AN/PDR-43 was 1.56 r/hr on the 0 to 5 r/hr range and did not appear on scale until H + 5 hours.

For the depth-dose ratemeter, the complete integration of the dose rate over the indicated period of time yielded a total dose of 75 r (Table 4.1). This gives a range of 25 to 53 percent greater than the minimum and maximum dose recorded by the 4-cm needles, a range of 34 to 53 percent greater than the shielded IM-107/PD's, and a range of 10 to 19 percent greater than the shielded DT-60/PD's.

The complete integration of the AN/PDR-43 rates yielded a total dose of 102 r, whereas the AN/PDR-44 integration showed a total dose of 119 r. A comparison with the 4-cm-needle doses among the racks and phantoms shows that the AN/PDR-43 read from 70 to 108 percent higher and that the AN/PDR-44 read from 98 to 143 percent higher. When the AN/PDR-43 integrated and scaled dose is compared with the unshielded IM-107/PD and DT-60/PD doses, values range from 62 to 89 percent and 33 to 44 percent higher, respectively.

Comparing the AN/PDR-44 integrated and scaled dose with the unshielded IM-107/PD and DT-60/PD doses, values ranging from 89 to 120 percent and 55 to 68 percent higher, respectively, are noted.

The integrated surface doses as predicted by the AN/PDR-43 and -44 appear to be in considerable error. In addition to the possible sources of error, such as energy-directional dependence and decreasing battery voltage, a possible calibration error may have existed (at least for the AN/PDR-43 and AN/PDR-44 radiacs). The scaling factor introduced to approximate the doses received by the dosimeters in Shot Hood was 3.24. Thus, it must be emphasized at this time that any error that existed in the calibration of the test ratemeters would have been magnified by the above scaling factor. Similarly, any error that may have been present in the calibration of the AN/PDR-43 that was used to monitor the 7 r/hr field would markedly effect the calculated dose as well.

4.4 LABORATORY WORK PERFORMED AND INDICATED

The large differences between the integrated ratemeter dose values and the total accumulated 4-cm-needle dose and both shielded and unshielded dosimeter dose were resolved as follows:

4.4.1 Standards. Upon the return to the laboratory, the ratemeter was repaired and recalibrated and found to agree within 10 percent with the imbedded needles for energies in the range 80 kev to 1.2 Mev. Thus, the greater variation encountered in the field is considered to be due to non-uniformity of field strength and geometrical conditions between ratemeter and dosimeter and rack phantoms and the errors inherent in the mathematical assumptions and extrapolation.

4.4.2 Energy-Directional Dependence. The scope and complexity of a complete study to determine the characteristics of energy-directional dependence of all the equipment evaluated by this project is presently being initiated by the Bureau of Ships (Bu Ships). Time and considerations made this study heretofore prohibitive, consequently this information is not available for inclusion in this report.

4.4.3 Additional Shielding Required. As previously mentioned, laboratory studies conducted since the field tests have shown that selective shielding could be designed to reduce the higher energy response of the DT-60/PD dosimeter. The actual design of ratemeter-detector shields was not an objective of Project 2.8, but comparison readings with a depth dose standard were. The results show that shielding is required. The development of suitable shields will be undertaken as part of Operation Trumpet.

Chapter 5
CONCLUSIONS and RECOMMENDATIONS

5.1 CONCLUSIONS

The 0.060-inch stainless-steel shielding used for the IM-107/PD dosimeters reduces response of the IM-107/PD's to the point where correlation within 6 percent of the 4-cm depth dose for both neutron-induced and fallout fields is achieved.

The 0.012-inch lead shielding on the DT-60/PD dosimeters reduces their response so that readings (uncorrected for temperature effects) of 22 to 34 percent higher than the 4-cm-depth dose are obtained for both induced and fallout fields. If temperature corrections are made, the variation in response is reduced to 17 to 29 percent. It is considered that additional shielding (based on laboratory experiments) could be designed to better correlate DT-60/PD response with depth-dose readings.

The data obtained show that both the AN/PDR-44(XN-1) ratemeters will result in a considerably high estimate of dose, if the depth dose is considered the standard. Shielding of the ratemeters is indicated.

5.2 RECOMMENDATIONS

If correlation of surface dose with depth dose is desired, future procurement specifications for IM-107/PD dosimeters should incorporate an additional 0.060-inch stainless-steel wall around the sensitive volume.

For the DT-60/PD dosimeters, heavier shielding (0.020 inch of lead), suitably compensated for energy dependence should be thoroughly investigated under laboratory conditions.

The development of suitable ratemeter shields should be undertaken in the laboratory work preceding the field work of Operation Trumpet.

REFERENCES

1. E.P. Cronkite and V.P. Bond; "Effects of Radiation on Mammals"; Review of Physiology, Vol 18, Pages 483–526; 1956; Unclassified.

2. Samuel C. Rainey and James W. Duckworth; "Evaluation of Standard Navy Dosimeters DT-60/PD and IM-107/PD in Residual Radiation Fields Aboard Ships"; Project 2.72, Operation Redwing, ITR-1350, July 1956; Bureau of Ships, Washington, D.C.

3. George W. Imirie, Jr. and Robert Sharp; "Radiation Energy Absorbed by Human Phantoms in a Fission Fallout Field"; Project 2.6, Operation Teapot, WT-1120, May 1955; U.S. Naval Medical Research Institute, Bethesda, Maryland; Confidential Restricted Data.

4. National Bureau of Standards Handbook, No. 59; "External Radiation Hazards"; September 1954; Unclassified.

5. F.W. Chambers and others; "Residual Ionizing Radiation Depth Dose Measurements in Unit-Density Material"; Project 2.2b, Operation Upshot-Knothole, WT-719, February 1957; Naval Medical Research Institute, Bethesda, Maryland; Confidential Restricted Data.

6. F.W. Spiers; "Materials for Depth-Dose Measurement"; British J. Radiol. 16:90, 1943; Unclassified.

7. Frank Day; National Bureau of Standards unpublished data; Unclassified.

8. "Military Aspects of the Biological Effects of Radiation"; AFSWP-611; 9 November 1956; Berlin, New York; Secret Restricted Data.

9. Bureau of Ships Instruction Book for Radiac Set AN/PDR-43 (XN-1); Contract NObsr. 71163; Unclassified.

10. Bureau of Ships Contract Specification for Radiac Set AN/PDR-44 (XN-1); SHIPS-R-2047 of 1 August 1955; Unclassified.

11. J. Schulman; "Radiophotoluminescence Dosimetry of the United States Navy"; Nucleonics, Vol II, No. 10, Pages 52–56; October 1953; Unclassified.

12. George A. Work; "Accuracy of Military Radiacs"; Project 6.1.2, Operation Teapot, WT-1138, November 15, 1957; U.S. Naval Radiological Defense Laboratory, San Francisco 24, California; Official Use Only.

13. A.E. Cohen and others; "Evaluation of New Types of Radiac Instruments"; Project 2.6, Operation Plumbbob, ITR-1415, October 18, 1957; U.S. Army Signal Engineering Laboratories, Fort Monmouth, New Jersey; Secret Restricted Data.

DISTRIBUTION

Military Distribution Categories 22 and 42

ARMY ACTIVITIES

1 Deputy Chief of Staff for Military Operations, D/A, Washington 25, D.C. ATTN: Dir. of SW&R
2 Chief of Research and Development, D/A, Washington 25, D.C. ATTN: Atomic Div.
3 Assistant Chief of Staff, Intelligence, D/A, Washington 25, D.C.
4- 5 Chief Chemical Officer, D/A, Washington 25, D.C.
6 Chief of Engineers, D/A, Washington 25, D.C. ATTN: ENGNB
7 Chief of Engineers, D/A, Washington 25, D.C. ATTN: ENGEB
8 Chief of Engineers, D/A, Washington 25, D.C. ATTN: ENGTB
9- 10 Office, Chief of Ordnance, D/A, Washington 25, D.C. ATTN: ORDTN
11 Chief Signal Officer, D/A, Comb. Dev. and Ops. Div., Washington 25, D.C. ATTN: SIGCO-4
12 Chief of Transportation, D/A, Office of Planning and Int., Washington 25, D.C.
13 The Surgeon General, D/A, Washington 25, D.C. ATTN: MEDNE
14- 16 Commanding General, U.S. Continental Army Command, Ft. Monroe, Va.
17 Director of Special Weapons Development Office, Headquarters CONARC, Ft. Bliss, Tex. ATTN: Capt. Chester I. Peterson
18 President, U.S. Army Artillery Board, Ft. Sill, Okla.
19 President, U.S. Army Air Defense Board, Ft. Bliss, Tex.
20 President, U.S. Army Aviation Board, Ft. Rucker, Ala. ATTN: ATBG-DG
21 Commandant, U.S. Army Command & General Staff College, Ft. Leavenworth, Kansas. ATTN: ARCHIVES
22 Commandant, U.S. Army Air Defense School, Ft. Bliss, Tex. ATTN: Command & Staff Dept.
23 Commandant, U.S. Army Armored School, Ft. Knox, Ky.
24 Commandant, U.S. Army Artillery and Missile School, Ft. Sill, Okla. ATTN: Combat Development Department
25 Commandant, U.S. Army Aviation School, Ft. Rucker, Ala.
26 Commandant, U.S. Army Infantry School, Ft. Benning, Ga. ATTN: C.D.S.
27 Commandant, The Quartermaster School, U.S. Army, Ft. Lee, Va. ATTN: Chief, QM Library
28 Commandant, U.S. Army Ordnance School, Aberdeen Proving Ground, Md.
29 Commandant, U.S. Army Ordnance and Guided Missile School, Redstone Arsenal, Ala.
30 Commanding General, Chemical Corps Training Comd., Ft. McClellan, Ala.
31 Commandant, USA Signal School, Ft. Monmouth, N.J.
32 Commandant, USA Transport School, Ft. Eustis, Va. ATTN: Security and Info. Off.
33 Commanding General, The Engineer Center, Ft. Belvoir, Va. ATTN: Asst. Cmdt, Engr. School
34 Commanding General, Army Medical Service School, Brooke Army Medical Center, Ft. Sam Houston, Tex.
35 Director, Armed Forces Institute of Pathology, Walter Reed Army Med. Center, 625 16th St., NW, Washington 25, D.C.
36 Commanding Officer, Army Medical Research Lab., Ft. Knox, Ky.
37 Commandant, Walter Reed Army Inst. of Res., Walter Reed Army Medical Center, Washington 25, D.C.
38- 39 Commanding General, Qm R&D Comd., QM R&D Cntr., Natick, Mass. ATTN: CBR Liaison Officer
40 Commanding General, U.S. Army Chemical Corps, Research and Development Comd., Washington 25, D.C.
41 Commanding Officer, Chemical Warfare Lab., Army Chemical Center, Md. ATTN: Tech. Library
42 Commanding General, Engineer Research and Dev. Lab., Ft. Belvoir, Va. ATTN: Chief, Tech. Support Branch
43 Director, Waterways Experiment Station, P.O. Box 631, Vicksburg, Miss. ATTN: Library
44 Commanding Officer, Office of Ordnance Research, Box CM, Duke Station, Durham, North Carolina
45 Commanding Officer, Picatinny Arsenal, Dover, N.J. ATTN: ORDBB-TK
46 Commanding Officer, Diamond Ord. Fuze Labs., Washington 25, D.C. ATTN: Chief, Nuclear Vulnerability Br. (230)
47- 48 Commanding General, Aberdeen Proving Grounds, Md. ATTN: Director, Ballistics Research Laboratory
49 Commanding General, Frankford Arsenal, Bridge and Tacony St., Philadelphia, Pa.
50- 51 Commanding General, U.S. Army Ord. Missile Command, Redstone Arsenal, Ala.
52 Commander, Army Rocket and Guided Missile Agency, Redstone Arsenal, Ala. ATTN: Tech Library
53 Commanding General, White Sands Proving Ground, Las Cruces, N. Mex. ATTN: ORDBS-OM
54 Commander, Army Ballistic Missile Agency, Redstone Arsenal, Ala. ATTN: ORDAB-HT
55 Commanding Officer, Ord. Materials Research Off., Watertown Arsenal, Watertown 72, Mass. ATTN: Dr. Foster
56 Commanding General, Ordnance Tank Automotive Command, Detroit Arsenal, Centerline, Mich. ATTN: ORDMC-RO
57 Commanding Officer, USA Signal R&D Laboratory, Ft. Monmouth, N.J.
58 Commanding General, U.S. Army Electronic Proving Ground, Ft. Huachuca, Ariz. ATTN: Tech. Library
59 Commanding General, USA Combat Surveillance Agency, 1124 N. Highland St., Arlington, Va.
60 Commanding Officer, USA, Signal R&D Laboratory, Ft. Monmouth, N.J. ATTN: Tech. Doc. Ctr., Evans Area
61 Director, Operations Research Office, Johns Hopkins University, 6935 Arlington Rd., Bethesda 14, Md.
62 Commandant, U.S. Army Chemical Corps, CBR Weapons School, Dugway Proving Ground, Dugway, Utah.
63 Commanding General, U. S. ORD Special Weapons-Ammunition Command, Dover, N.J.
64 Commander-in-Chief, U.S. Army Europe, APO 403, New York, N.Y. ATTN: Opot. Div., Weapons Br.
65 Commanding Officer, 9th Hospital Center, APO 180, New York, N.Y. ATTN: CO, US Army Nuclear Medicine Research Detachment, Europe

NAVY ACTIVITIES

66 Chief of Naval Operations, D/N, Washington 25, D.C. ATTN: OP-03EG
67 Chief of Naval Operations, D/N, Washington 25, D.C. ATTN: OP-75
68 Chief of Naval Operations, D/N, Washington 25, D.C. ATTN: OP-91
69 Chief of Naval Operations, D/N, Washington 25, D.C. ATTN: OP-922G2
70 Chief of Naval Personnel, D/N, Washington 25, D.C.
71- 72 Chief of Naval Research, D/N, Washington 25, D.C. ATTN: Code 811
73- 74 Chief, Bureau of Aeronautics, D/N, Washington 25, D.C.
75 Chief, Bureau of Medicine and Surgery, D/N, Washington 25, D.C. ATTN: Special Wpns. Def. Div.
76 Chief, Bureau of Ordnance, D/N, Washington 25, D.C.
77 Chief, Bureau of Ordnance, D/N, Washington 25, D.C. ATTN: S.P.
78 Chief, Bureau of Ships, D/N, Washington 25, D.C. ATTN: Code 423
79 Chief, Bureau of Yards and Docks, D/N, Washington 25, D.C. ATTN: D-440
80 Director, U.S. Naval Research Laboratory, Washington 25, D.C. ATTN: Mrs. Katherine H. Cass
81- 82 Commander, U.S. Naval Ordnance Laboratory, White Oak, Silver Spring 19, Md.

83 Director, Material Lab. (Code 900), New York Naval Shipyard, Brooklyn 1, N.Y.
84 Commanding Officer and Director, Navy Electronics Laboratory, San Diego 52, Calif.
85 Commanding Officer, U.S. Naval Mine Defense Lab., Panama City, Fla.
86- 89 Commanding Officer, U.S. Naval Radiological Defense Laboratory, San Francisco, Calif. ATTN: Tech. Info. Div.
90- 91 Commanding Officer and Director, U.S. Naval Civil Engineering Laboratory, Port Hueneme, Calif. ATTN: Code L31
92 Commanding Officer, U.S. Naval Schools Command, U.S. Naval Station, Treasure Island, San Francisco, Calif.
93 Superintendent, U.S. Naval Postgraduate School, Monterey, Calif.
94 Officer-in-Charge, U.S. Naval School, CEC Officers, U.S. Naval Construction Bn. Center, Port Hueneme, Calif.
95 Commanding Officer, Nuclear Weapons Training Center, Atlantic, U.S. Naval Base, Norfolk 11, Va. ATTN: Nuclear Warfare Dept.
96 Commanding Officer, Nuclear Weapons Training Center, Pacific, Naval Station, San Diego, Calif.
97 Commanding Officer, U.S. Naval Damage Control Tng. Center, Naval Base, Philadelphia 12, Pa. ATTN: ABC Defense Course
98 Commanding Officer, Air Development Squadron 5, VX-5, China Lake, Calif.
99 Commander, Officer U.S. Naval Air Development Center, Johnsville, Pa. ATTN: NAS, Librarian
100 Commanding Officer, U.S. Naval Medical Research Institute, National Naval Medical Center, Bethesda, Md.
101 Officer-in-Charge, U.S. Naval Supply Research and Development Facility, Naval Supply Depot, Bayonne, N.J.
102-105 Commandant, U.S. Marine Corps, Washington 25, D.C. ATTN: Code A03H
106 Chief, Bureau of Ships, D/N, Washington 25, D.C. ATTN: Code 372
107 Commanding Officer, U.S. Naval CIC School, U.S. Naval Air Station, Glynco, Brunswick, Ga.
108 Chief of Naval Operations, Department of the Navy, Washington 25, D.C. ATTN: OP-25

AIR FORCE ACTIVITIES

109 Assistant for Atomic Energy, HQ, USAF, Washington 25, D.C. ATTN: DCS/O
110 Deputy Chief of Staff, Operations HQ. USAF, Washington 25, D.C. ATTN: Operations Analysis
111-112 Assistant Chief of Staff, Intelligence, HQ. USAF, Washington 25, D.C. ATTN: AFCIN-3A2A
113 Director of Research and Development, DCS/D, HQ. USAF, Washington 25, D.C. ATTN: Guidance and Weapons Div.
114 The Surgeon General, HQ. USAF, Washington 25, D.C. ATTN: Bio.-Def. Pre. Med. Division
115 Commander, Tactical Air Command, Langley AFB, Va. ATTN: Doc. Security Branch
116 Commander, Air Defense Command, Ent AFB, Colorado. ATTN: Assistant for Atomic Energy, ADLDC-A
117 Commander, Hq. Air Research and Development Command, Andrews AFB, Washington 25, D.C. ATTN: RDSWA
118 Commander, Air Force Ballistic Missile Div. HQ. ARDC, Air Force Unit Post Office, Los Angeles 45, Calif. ATTN: WDSOT
119-120 Commander, AF Cambridge Research Center, L. G. Hanscom Field, Bedford, Mass. ATTN: CRQST-2
121-125 Commander, Air Force Special Weapons Center, Kirtland AFB, Albuquerque, N. Mex. ATTN: Tech. Info. & Intel. Div.
126-127 Director, Air University Library, Maxwell AFB, Ala.
128 Commander, Lowry AFB, Denver, Colorado. ATTN: Dept. of Sp. Wpns. Tng.
129 Commandant, School of Aviation Medicine, USAF, Randolph AFB, Tex. ATTN: Research Secretariat
130 Commander, 1009th Sp. Wpns. Squadron, HQ. USAF, Washington 25, D.C.
131-132 Commander, Wright Air Development Center, Wright-Patterson AFB, Dayton, Ohio. ATTN: WCOSI
133-134 Director, USAF Project RAND, VIA: USAF Liaison Office, The RAND Corp., 1700 Main St., Santa Monica, Calif.
135 Commander, Air Defense Systems Integration Div., L. G. Hanscom Field, Bedford, Mass. ATTN: SIDE-S
136 Chief, Ballistic Missile Early Warning Project Office, 220 Church St., New York 13, N.Y. ATTN: Col. Leo V. Skinner, USAF
137 Commander, Air Technical Intelligence Center, USAF, Wright-Patterson AFB, Ohio. ATTN: AFCIN-4Bla, Library
138 Assistant Chief of Staff, Intelligence, HQ. USAFE, APO 633, New York, N.Y. ATTN: Directorate of Air Targets
139 Commander-in-Chief, Pacific Air Forces, APO 953, San Francisco, Calif. ATTN: PFCIE-MB, Base Recovery

OTHER DEPARTMENT OF DEFENSE ACTIVITIES

140 Director of Defense Research and Engineering, Washington 25, D.C. ATTN: Tech. Library
141 Director, Weapons Systems Evaluation Group, Room 1E880, The Pentagon, Washington 25, D.C.
142-145 Chief, Defense Atomic Support Agency, Washington 25, D.C. ATTN: Document Library
146 Commander, Field Command, DASA, Sandia Base, Albuquerque, N. Mex.
147 Commander, Field Command, DASA, Sandia Base, Albuquerque, N. Mex. ATTN: FCTG
148-152 Commander, Field Command, DASA, Sandia Base, Albuquerque, N. Mex. ATTN: FCWT
153 Commander, JTF-7, Arlington Hall Station, Arlington 12, Va.
154 Administrator, National Aeronautics and Space Administration, 1520 "H" St., N.W., Washington 25, D.C. ATTN: Mr. R. V. Rhode
155 Commander-in-Chief, Strategic Air Command, Offutt AFB, Neb. ATTN: OAWS
156 Commandant, US Coast Guard, 1300 E. St., N.W., Washington 25, D.C. ATTN: (OIN)
157 Commander-in-Chief, EUCOM, APO 128, New York, N.Y.

ATOMIC ENERGY COMMISSION ACTIVITIES

158-160 U.S. Atomic Energy Commission, Technical Library, Washington 25, D.C. ATTN: For DMA
161-162 Los Alamos Scientific Laboratory, Report Library, P.O. Box 1663, Los Alamos, N. Mex. ATTN: Helen Redman
163-167 Sandia Corporation, Classified Document Division, Sandia Base, Albuquerque, N. Mex. ATTN: H. J. Smyth, Jr.
168-170 University of California Lawrence Radiation Laboratory, P.O. Box 808, Livermore, Calif. ATTN: Clovis G. Craig
171 Essential Operating Records, Division of Information Services for Storage at NRC-H. ATTN: John E. Hans, Chief, Headquarters Records and Mail Service Branch, U.S. AEC, Washington 25, D.C.
172 Weapon Data Section, Technical Information Service Extension, Oak Ridge, Tenn.
173-205 Technical Information Service Extension, Oak Ridge, Tenn. (Surplus)

AEC Technical Information Service Extension
Oak Ridge, Tennessee